UNITED NATIONS EDUCATIONAL, SCIENTIFIC AND CULTURAL ORGANIZATION
INTERNATIONAL ATOMIC ENERGY AGENCY
INTERNATIONAL CENTRE FOR THEORETICAL PHYSICS
I.C.T.P., P.O. BOX 586, 34100 TRIESTE, ITALY, CABLE: CENTRATOM TRIESTE

SMR/989 - 27

"Course on Shallow Water and Shelf Sea Dynamics"
7 - 25 April 1997

"Toward a Mediterranean Coupled Model of the Nitrogen Cycle"

R. MOSETTI
Osservatorio Geofisico Sperimentale
Borgo Grotta Gigante (Trieste)
Italy

Please note: These are preliminary notes intended for internal distribution only.

Toward a Mediterranean coupled model of the nitrogen cycle

Alessandro Crise, Guido Crispi and Elena Mauri
Osservatorio Geofisico Sperimentale, P.O.Box 2011, 34016 Trieste, Italy

The Oceanography Society meeting
Amsterdam 7-11 July 1996

1 Abstract

The general circulation horizontal and vertical processes interact with the biogeochemical cycles at proper scales: in this study the lower trophic level variability induced by physical forcings in the Mediterranean is investigated by means of a 3D coupled hydrodynamical ecological model.

The trophic dynamics are described using an aggregated model based on inorganic nitrogen, phytoplankton and detritus.

The seasonal cycle shows marked spatial differences according to the prevailing cyclonic or anticyclonic regime, creating zonal and meridional permanent trophic gradients. The open ocean ecosystem response is moreover influenced by coastal boundaries/open ocean exchanges and by Ekman suction enrichment.

This leads to the tentative conclusion that the upper thermocline circulation determines directly or indirectly the distribution of the dissolved inorganic nitrogen concentration. This is supported by the comparison with CZCS images.

2 Introduction

This brief presentation outlines some of the results obtained with a coupled three-dimensional model of the nitrogen cycle in the Mediterranean Sea.

The rationale of using a three-dimensional model emerges considering the influence for the nutrients dynamics of horizontal transport, of upwelling/downwelling processes and of vertical mixing; moreover the importance for the Mediterranean ecosystem of the Gibraltar inflow/outflow as an inverse estuarine mechanism; and also the spatial distribution and the seasonal variability of the physical forcings for phytoplankton growth. In consequence the sinking and the remineralization of the particulate matter must be followed with detail at the sub-basin scale.

3 Numerical approach

The aggregated trophodynamic nitrogen model used is described by N,P, and D (Crise et al, 1995). N represents the dissolved inorganic nitrogen, P is the phytoplankton biomass nitrogen equivalent and D those organic forms from DON to the detritus plus epibacteria aggregates.

An estimation of detritus sinking velocity for the particulate organic form was made according with weighted averages of reported vertical settling velocities for different fraction of D.

In terms of vertical transport, the falling particles can be operationally grouped into three categories: fecal pellets, aggregates, and dissolved organic matter (at least the labile part should be taken into account). This fraction gives a small contribution to the gravity driven D flux because of their neutral buoyancy.

These fractions have different remineralization rates, depending on external conditions (temperature, pressure) and the ultimate fate of the nitrogen content is influenced by the recycling many times in the productive zone under different states before the sinking. Nevertheless, using averaged literature data for all those D forms, a regeneration time scale of ten days was obtained and a averaged sinking velocity of 5 meters/day was estimated.

A correct estimate of nitrogen fluxes needs a realistic initialization of the DIN; since nitrates are by far the largest fraction of DIN (at least in the ocean interiors) the DIN was initialized with nitrates vertical profiles typical of each subbasin. This stepwise initializing function was smoothed using a 3x3 moving average filtering.

The profile of the phytoplanktonic biomass used for initialization of the model is worked out from the Chlorophyll a measured in the Ionian Sea during the cruise POEM-BC-O91 in October 1991.

The detritus initial profile is chosen null everywhere. After the spin-up it reaches its quasistationary equilibrium inside the basin.

To correctly simulate the nitrogen inflow/outflow at the Gibraltar Strait a representation of the nutrient exchanges is implemented using an Atlantic box extending from 5.5 W to 9.5W. In this buffer zone a relaxation to proper surface experimental values for all the three state variables is imposed.

For the relaxation of nitrate in the Atlantic box of the model we considered the data from the ATLANTIS II cruise. For phytoplankton the same profile used for initialization inside the basin is considered for relaxation in the buffer zone. The relaxation to zero of the detritus is chosen in all the Atlantic zone, with a time constant of 5 days, as the other variables.

For the surface relaxation boundary condition in the Mediterranean basin, the surface value of the initial profile of phytoplankton is relaxed with a time constant of 5 days also; to mantain the

nitrogen content a balancing term in the detritus compartment is introduced.

Using staggered finite differences it is possible to have negative concentrations where strong lateral or vertical gradients are present this wiggling effect is overcome here with a borrowing technique. This technique has the advantage of conservating the overall nitrogen inside the basin.

The simulation experiments were planned in order to obtain a quasi repeating cycle, running firstly the hydrodynamics for five years. This spinup time is chosen as a compromise between the asymptothic convergence ot the kinetic energy and the progressive vertical structure erosion induced by the diffusive processes. After the spinup time the whole coupled model is run at least for 3 years: this time seems to be enough to reproduce a seasonal cycle in the upper layer.

4 Simulation results

4.1 Model runs, spinup and quasi repeating cycle

The simulation experiments were planned so as to obtain a quasi-repeating cycle. The MOM-based primitive equation model (Pinardi et al., 1993; Roussenov et al., 1995) is run first to obtain the spinup of the hydrodynamics. The version used in this paper, hereafter called PE4L31, has a spatial discretization of 1/4 degree horizontally and 31 levels vertically. The subgrid turbulence parametrization adopted in this work is $0.4\,10^{19} cm^4 s^{-1}$ as biharmonic horizontal eddy viscosity, and $1.5\ cm^2 s^{-1}$ for the vertical viscosity, while $0.2\,10^{19} cm^4 s^{-1}$ and $0.3\ cm^2 s^{-1}$ are respectively the biharmonic horizontal and vertical diffusions.

The spinup of PE4L31 is five years with a timestep of 2400s, chosen as a compromise between asymptotic convergence of the kinetic energy and progressive vertical structure erosion induced by the diffusive processes. After the spinup time the whole coupled model is run for at least 3 years. This time seems enough to reproduce a seasonal cycle in the upper layer. A summary of the most important numerical experiments is presented in table 1 .

The first observation to make is that the improvements are focussed basically on the ecological part. An exception is run b11 which uses higher horizontal eddy viscosity and diffusivity. In fig. 1 the relative effects of model sensitivity to the incremental parameter variation are presented in a scatter plot form: in the case of linear covaring variables the scatter plot is supposed to lie on a straight line.

Two reference levels were chosen to see the differences in model response: one at 100m depth, where the DIN concentration begins

Run	PE4L31 Model	NPD Model
b8.1	standard	standard with $w_D = 0.$
b9.567	standard	standard
b10.5678	standard	standard with w_D =0.0058 cms^{-1} and r = $1.1810^{-6}s^{-1}$
b11.567	A_h =.8 10^{19}	as b10.5678 with K_h =.4 10^{19}
b14.567	standard	as b10.567 with improved light model

Table 1: Selected numerical experiments with PE4L31-NPD coupled model The hydrodynamics has a spinup time of 5 years. The duration of the each biological run after the fifth year is indicated in the postfix of each run name. Each run is identified by the key modifications introduced in that run.

to be evident, and the other at 300m depth, below the direct effect of the productive layer, and different markers are used to identify the subbasins. The effects of the enhanced vertical flux of the detritus (run b10) are evident in the increment in DIN concentration both at 100m (fig. 1.c) and 300m (fig. 1.f) for the Western Mediterranean. The Ionian Sea does not present a significant mean variation while the Levantine seems to be more nutrient depleted.

If higher horizontal viscosity and diffusivity are introduced (run b11) the shape of the scatter plot is basically the same, but the marker cloud is much more scattered, both at 100m and 300m (fig. 1.b and 1.e respectively). The spreading is present in all the basins, stronger in the upper level and more pronounced for low concentrations. This effect can be related to the basin-wide constant parametrization of eddy viscosity and diffusivity. The effect of the space-variant cloud-dependent light model has the effect of reducing high concentrations, and this is particularly true at 300m (fig.1.d). This is definitely not a direct effect on phytoplankton uptake because the productive layer is shallower in the Western Mediterranean (where the differences are higher) in b14 than in b9. Instead a reduction in solar irradiance during the most productive period (late winter - early spring) reduces the downward fluxes of detritus, limiting the increment of remineralized DIN.

In conclusion, the vertical detritus fluxes seem to play a major role in maintaining the vertical nutrient gradient. Here we will discuss in particular the results obtained in run b14, which is considered the most detailed in the parametrization of physical forcings and biological response, and all the examples will be referred to this run unless otherwise stated.

4.2 Nitrogen budgets

In tab. 2 are reported the total nitrate budgets in the Gibraltar and Sicily straits after the first year of simulation. All the numerical ex-

Nitrate concentrations	Water fluxes	Gibraltar	Sicily
(Coste, 1988)	(Lacombe, 1971)	−2.17	-
(Coste, 1988; 1971)	(Bethoux, 1979)	−3.11	−1.57
(Coste, 1988)	(Bryden et al., 1988)	−1.57	-
(Coste, 1988; 1971)	(Sarmiento et al., 1988)	−1.25	−.91
(Coste, 1988; 1971)	(Harzallah et al., 1993)	−1.41	−.85
RUN8	PE4L31	−1.73	−.51
RUN9	PE4L31	−1.78	−.63
RUN10	PE4L31	−2.74	−1.85
RUN11	PE4L31	−3.63	−2.00
RUN14	PE4L31	−2.50	−1.70

Table 2: Yearly nitrate outflow at Gibraltar and Sicily straits ($10^6 tons/year$). The model results are the total outflows after the first year of simulation.

periments were obtained with the same physical submodel. These results are compared with some estimates obtained in terms of water fluxes and using the nitrate mean concentrations in the inflow and outflow water masses. For nitrate concentrations in the Gibraltar Strait, an inflow mean concentration of $4.0 mgatN/m^3$ and an outflow of $8.6 mgatN/m^3$ are used. For the Sicily Strait the estimate of $4.0 mgatN/m^3$ for the outflow water concentration is used, while for the inflow an upper value of $1.0 mgatN/m^3$ is held fixed.

The model results are in keeping with the budget estimate ranges here considered. Our lowest results were obtained using no sinking rates (run b8). This is due to the fact that in this run we did not have any mechanism to pump the matter down. Considering a sinking rate of $1m/day$ (run b9), an increased loss at the strait is obtained. This result is magnified by a further increase in the sinking rate and regeneration time (run b10), suggesting that this could be a good choice for calibration of the overall model. Also the introduction of a variable penetration light coefficient diminishes the exchanges and this is due to lower biological activity in particular in the western part of the basin.

4.3 Climatology

As a climatological synopsis of the trophic response to physical forcings in the Mediterranean Sea we present a comparison between the streamfunction and the nutrient distribution below the euphotic zone. Fig. 2.a represents the annual mean total transport streamfunction ψ expressed in Sv; the centers of the anticyclones and the cyclones are identified respectively by positive and negative values. The model reproduces the well known permanent cyclonic patterns in the Gulf of Lions, in the Thyrrenian, and in the Levantine Basin.

The Algerian current is represented by the presence of an unstable coastal front that on average exibits an energetic sequence of cyclonic and anticyclonic gyres. In the Ionian Sea we find that the circulation is basically anticyclonic, but the center of the basin is directly influenced by a wind-driven cyclonic gyre. The Levantine basin is influenced by the large cyclonic area connected with the Rhodes gyre, with the noticeable exception of the anticyclone offshore from the Israeli coast.

If we compare the above maxima and minima positions with the maxima in DIN concentration at 140m depth (2.b), where no primary production is present, we see that there is a strong correlation between the high nutrient concentration spots and cyclonic areas in the open sea, while coastal effects such as upwellings and coastal boundary currents are the prevailing processes in importing nutrients into areas such as the Spanish coast of the Alboran Sea, the Sicily and Calabria coasts, and the Algerian current. On the contrary, the effect of the anticyclonic areas on the DIN distribution is less evident in the upper layer because the Ekman pumping in an anticyclonic vortex deepens the nutrient depleted layer, advecting water laterally in the upper layer. This effect can increase the spreading of coastal upwellings and possibly contributes to a remote control of the straits regime (in particular in the Ionian sea).

The permanent cyclonic gyres in the Gulf of Lions and in the Rhodes area create isopycnal domes that carry nutrients into the euphotic zone, substaining the nutrient maxima reproduced by the model. This effect is also present in the Thyrrenian, but is much smoother.

In order to give a comprehensive view of the correlation between general circulation and DIN distribution, we plotted in fig 3 the streamfunction versus nutrient concentration at different depths using light grey for the Levantine Basin, dark grey for the Gulf of Lions(lb and gl in the figure) and black markers for the rest of the Mediterranean.

In fig 3.a we see that at 40m depth there is virtually no effect of the circulation on nutrient distribution and the highest maxima are present in proximity to $\psi = 0$, a condition found along the coasts, suggesting that the upwelling areas could be the main origin of this maximum. This effect is present, with different intensities in all the plots in fig. 3.

Neither the Levantine nor the Gulf of Lions present a specific response to the cyclonic circulation: this can be explained by the fact that the phytoplankton uptake is fast and virtually all new nutrient inputs are transformed into new production.

At 100m depth (3.b) we observe a much more scattered distribution and this is due to two concurring causes: firstly the progressive increase in nutrient concentration with depth extends the dynamic

range of DIN and, secondly, around this level we find the deep chlorophyll maximum (DCM) in the Levantine basin, while the Western Mediterranean has a shallower euphotic zone. In the latter case the phytoplankton uptake in not present and the nutrient distribution is affected only by the physical dynamics and by the remineralization processes. A clear influence of the circulation is therefore expected. The results confirm these speculations: the Levantine Basin has a distribution similar to the previous case while in the Gulf of Lions the effect of the cyclonic regime begins to be detectable. The anticyclonic circulation does not seem to affect nutrient distribution coherently and this supports the above considerations.

At 180m and 300m depth (figs. 3.c and 3.d) we find similar patterns for the basin overall, and in particular no specific influence of the anticyclonic circulation, or dependence of DIN concentration on circulation intensity in both the considered cyclonic areas.

The distributions in the *lb* and *gl* areas are between the axis $\psi = 0$ and a maximum value proportional to ψ intensity. This effect could be related to homogenization in vortices summed with the diffusion introduced to parametrize the subgrid scale mixing effects, the two processes thus working to smooth the DIN gradient induced by circulation. As a net effect we find similar DIN concentrations in the neighbourhoods of the cyclonic gyres even in the presence of high ψ gradients.

4.4 Seasonal cycle

The trophic seasonal variability in the Mediterranean seems to mitigate the chronic oligotrophy that affects this basin, as seen in fig. 4.a. In the upper layer where the effect of Ekman suction is stronger we see that, despite highly different concentrations in the eastern and western basins, in February, the mixing induced by wind stirring and by convective adjustment during the winter season create large areas with relatively higher nutrient availability.

The Liguro-Provenzal Sea and the Catalan Sea seem to be particularly involved in these processes with a southern zonal front roughly corresponding to the Balearic Front. Strong wind driven upwellings are present at the northern coast of the Alboran Sea and along the Provenzal and Catalan coasts. In the Alboran Sea there is a signature of fronts produced by the Western and Eastern (weaker) Alboran Gyres. The Mediterranean water flowing along the Spanish coast, enriched in nutrients by coastal processes, exibits higher nitrate concentrations than the surface Atlantic water at the same level. This is in accord with the ALMOFRONT 1 experimental results. The prevailing north-westerly winds create upwelling along the south-western Sicily coast and along the Calabrian coast. The Levantine Basin attains its highest DIN concentration in this

month, possibly because of the dense water formation and the instability that eventually generate a vertical homogeneization dragging on the surface nutrients present at depth. There is also an increased concentration of DIN in the side lobes of the Rhodes Gyre.

In June (4.b) the difference between the two main subbasins is striking and can be related to the different regimes at this level: in the Eastern Mediterranean the nutrient limitation is stronger, because an earlier developed and more stratified seasonal thermocline decouples the upper layer from the ocean interiors, and prevents the input of turbulent energy below the mixed layer.

The above considerations are not valid for the western basin: in this area the light extinction coefficient is higher and the euphotic zone is shallower. In general the Western Mediterranean exibits a more energetic distribution of nutrients induced by the wind stress in coastal areas and by the local circulation (Alboran Gyres). High DIN concentrations are present in the Liguro-Provenzal Basin, maintaining the meridional DIN gradient in this area. The wind driven upwelling offshore from the southern Sicily coast is still present.

In September (4.c) the nutrient depletion is still stronger and the map shows a very similar situation to June, with the exception that the Liguro-Provenzal nutrient concentration is almost homogeneous. In December (4.d) the wind and thermohaline forcings cooperate in breaking the thermocline in the western basin, with subsequent mixing; this is not true for the Eastern Mediterranean where late summer conditions are still present. In the Gulf of Lions, small concentrations indicate the weak convective adjustments that are only able to mix the upper layer.

In this season the Algerian Current seems to be more energetic but its contribution in terms of nutrients is negligeable. The Ionian Sea however seems to be nearer to winter conditions when increased nutrient availability is present, in particular in the northern part of the basin.

In fig. 5 the DIN distribution at 180m is presented. In February the signature of the vertical homogeneization in the Liguro-Provenzal Basin and in the Cretan Passage is seen by comparing figs. 5.a and 4.a: we notice at these two sites that the same area has the same DIN concentration (darker in fig. 4.a and lighter in fig. 5.a). The intense vertical export of nutrients from ocean interiors and the enhanced wind driven circulation determine a patchy trophic distribution.

During the early summer and late autumn periods, a progressive DIN replenishment occurs, finally producing a nutrient pool for the next winter mixing period. In this process the vertical flux induced by the detritus sinking can be estimated, showing the difference in DIN concentration below the nitracline (180m) between the b9 and b10 runs (fig. 6), which differ for detritus sinking velocity and

remineralization rate parametrization. The b10 experiment allows higher nurient regeneration in depth, where higher primary production and higher standing stocks are present. This in turn allows the presence of a seasonally varying detritus vertical flux that induces fertilization of the layers below the nitracline during spring and summer, thus creating an enriched pool of biochemical energy. This forms a trophic cell able to capture the nitrogen forms and to maintain lateral inhomogeneities over time, even in the presence of intense lateral advection (as in the Alboran Sea).

4.5 Phytoplankton growth

The other point to consider is that the simulated phytoplankton growth reaches a quasistationary cycle after about one year of simulation. This signifies that the mean values not only of the biomass, but also of the production, stabilize.

Hovmoeller diagrams taken in representative stations show the differences among the different subbasins.

The station taken in the Ligurian Sea (fig. 7) at 44.25N 9E exhibits a seasonal cycle with a maximum in May of about $1.2 mgatNm^{-3}$ for the phytoplankton, while there is a decreasing toward a minimum of activity in the months of November and December. It is remarkable the less content in nitrogen of the euphotic zone due to the 5 m/day detritus sinking velocity and a a greater peak in phytoplankton at approximately 40 m.

The trend of a temporal series data measured in situ (Fabiano et al., 1984) is quite similar to the seasonal variation obtained by the model. In fact in the March samples of the data chlorophyll-a is homogeneous all over the water column until 170m depth with a maximum at 25m, while the results of the model indicate a maximum in April-May at 40m. In summer the DCM is present at 70m, and the model reproduces the maximum of biomass at that depth.

In the Provenzal Sea, 39N 6E, the biomass maximum (appr. $1.8 mgatNm^{-3}$) is recognizable in March (fig. 8). The depth of this maximum is also 50m as in the preceding case, but the dynamics of the nitrogen is here more energetic due to the Balearic front.

An experimental transect acquired in April (Coste et al., 1972) shows that the eastern side of the transect (42.5N 4-10E) is clearly separated by the western side by a strong discontinuity. This is evidenced also by the inorganic nitrogen model results (not shown), as well a less evident stratification suggesting an anticipation of the seasonal layering with respect to the climatology. We want to stress here that this comparison is made only with the data taken in the second half of the MEDIPROD I cruise, made in April, while the winter data, taken in the first half of the cruise, were used for initializing the model. Data do not present any deep chlorophyll

maximum (Jacques et al., 1973). The model reproduces the western intensification in the chlorophyll-a present in the data, showing also a discontinuity between the subsurface peak located around 4E and the relative maximum present in the centre of the transect.

In the Ionian Sea, 34N 19E, the maximum depth for the phytoplankton growth is about 70m with values of the order of $1.0 mgatNm^{-3}$ (fig. 9). The results of this run confirm the vanishing after 100m of the phytoplankton due to the recycling of the total nitrogen. This is in good accord with the fact, that in absence of lateral and vertical movements, there is a maximum, after which it is not possible a biological quasistationary cycle.

The behaviour of the Hovmoller in the Levantine basin at 34N 34E near the Israelian coast is very similar to the Ionian Sea one, with the very significant difference that the nutricline is at 50m due to the vertical dynamics (fig. 10). Thus here is visible the superposition of two effects: the first is the deeper phytoplankton maximum that goes from 70 m in the Ionian to 120 m in the Levantine, because of the light penetration; the second is the nonstationarity (the quasistationary cycle is obtained after 4 or 5 years of simulation) of this particular station in front of the Israel coast after only 3 years of biological evolution. The maximum of phytoplankton is here obtained at 120m (biomass about $0.5 mgatNm^{-3}$), in accord with the west-east tilting of the deep chlorophyll maximum.

In Ionian and Levantine seas the comparison is more difficult because of the lack of time series. The available profiles are related to different sites within the subbasins during different periods. In Levantine Sea the effect of the increased light extinction coefficient is evident (Berman et al., 1986).In fact the deep chlorophyll maximum sampled in situ is at a similar depth of the maximum of biomass given by the model. The trend of seasonal variation is approximately the same: there is a maximum in May-June as in measurements , but the increase of chlorophyll-a in depth is roughly reproduced. In Ionian Sea the structures recognized in the data (Rabitti et al., 1994) in late winter and late summer situations are well captured in the model (not shown) both in euphotic and in aphotic zones. Also the deep chlorophyll maximum at 75-80m is well reproduced by the model.

4.6 Surface chlorophyll

The result for the chlorophyll concentration in the first 20m is shown in fig. 11 for the April situation of the second year simulation. This is a reasonable choice because the optical length is about 15m in the Western and reaches approximately 30m in the Eastern Mediterranean.

A clear west-east gradient is evident with a maximum in the

Alboran Sea and in the Ligurian-Provenzal basin and a minimum in the Levantine Sea.

In particular the Alboran Sea anticyclonic circulation makes the Modified Atlantic Water flow along the Spanish coast toward the Balearic Sea.

In the Ligurian-Provenzal basin the strong effect of convection determines a well localized increase in biomass. Also the biological effects determined by upwelling along the south coast of Sardinia, Sicily and the south-east coast of Italy are evident.

Noticeable is the north-south gradient in the Ionian Sea, with higher values in the north and lower ones in the Sirte Gulf.

A strict comparison with data of these results cannot be attemped at the moment. These results give a proper description for the open ocean, but not yet for the coastal regions. The most important reason is that the terrestrial sources must be taken into account, as well as the shelf-open ocean processes and the benthic-pelagic coupling important in particular in the Adriatic and Aegean Seas.

Anyway considering the CZCS data (fig. 12), obtained averaging 8 years of images from 1978 to 1986, a significant correspondence can be noticed in the open ocean. The west-east gradient is evident and also the north-south gradients from the Ligurian to the Balearic Sea and in the Ionian Sea are well defined patterns of this late winter situation.

Also the numerical values are in good accord in the Western part of the basin, reaching a maximum of about $1.5 mg Chl m^{-3}$, while for the Eastern part greater values are obtained in the model results than in CZCS data for this period. In particular the Sicily and Sardinia upwellings seem to be overestimated in the model.

In October the model chlorophyll concentration is depleted and follows the circulation patterns with minima in the southern regions and in the Levantine basin and maxima in the Alboran Sea and in the Balearic Sea, also the Sicily coast is affected by the upwelling effects.

The comparison with the CZCS data of the same period is good in qualitative terms, giving always a clear west-east gradient and pronounced zonal structures, but the values, in particular in the eastern basin, are two times less with minima of the order of $0.05 mg Chl m^{-3}$. This can be due to the CZCS overestimation of the chlorophyll content, because of the processing of the signal comprising not only the biomass, but also the dead matter.

The late winter and late summer situations discussed above are, broadly speaking, confirmed by the situation in winter and summer (fig. 13).

In January the bloom of the first layer is evident in the model chlorophyll, in particular in the Western Mediterranean. This is due to the deep nitrogen apport induced by the winter mixing. The me-

andering of the Modified Atlantic Water is evident and also its flow along the African coast, because of the prevalent cyclonic regime in the Ionian Sea.

In July the summer depleted situation is almost reached, where the influence of the Atlantic Water is now more active in the Eastern basin, where the zonal distribution due to the circulation tends to stabilize.

The values are newly in good accord with the data (fig. 14), namely more in the northern part of the basin than in the south. The underestimation, clearly visible also here, can be explained with the presence, discussed above, of the dead organic matter, but with a less content than in the late summer situation.

5 Acknowledgments

This work was partially funded by the EC contract MAS2-CT93-0055. All the figures were obtained with the public domain package GrADS. Corresponding author mail address: crispi@rs2oga.ogs.trieste.it

6 References

- Berman, T., Azov, Y., Schneller, A., Walline, P. and Townsend, D.W., 1986. Extent, transparency, and phytoplankton distribution of the neritic waters overlying the Israeli coastal shelf, Oceanol. Acta, 9, 439-447.

- Coste, B., Gostan, J., et Minas, H.J., 1972. Influence des Conditions Hivernales sur les Productions Phyto- et Zooplanctoniques en Méditerranée Nord-Occidentale. I. Structures Hydrologiques et Distribution des Sels Nutritifs. Mar. Biol., 16; 320-348.

- Crise, A., Crispi, G., Mauri, E. and Mosetti, R., 1995. Seasonal variability of the nitrogen cycle in the Mediterranean Sea. Rapp. int. Mer Medit., 34, 11.

- Fabiano, M., Zavatarelli, M. and Palmero, S., 1984. Observations sur la matière organique particulaire (protéines, glucides, lipides, chlorophylle) en Mer Ligure. Téthis, 11(2), 133-140.

- Jacques, G., Minas, H.J., Minas, M. and Nival, P., 1973. Influence des conditions hivernales sur les produsctions phyto- et zooplanctoniques en Méditerranée nord-occidentale, II, Biomasse et production phytoplanctonique. Mar. Biol., 23, 251-265.

- Pinardi, N., Roether, W., Marshall, J., Lascaratos, A., Krestenitis, Y. and Haines, K., 1993. Mediterranean Eddy Resolving Modelling and Interdisciplinary Studies (Contract MAST 0039-C(A)). Final scientific and management Report, pp. 45.

- Rabitti, S., Civitarese, G. and Ribera, M., 1994. Data Report Cruise POEM-BC-October 1991 - Ionian Basin and Sicily Channel Part II: Chemical and Biological Data. Tech. Rep. No. 13/94 - CNR/IBM.

- Roussenov, V., Stanev, E., Artale, V. and Pinardi, N., 1995. A seasonal model of the Mediterranean Sea general circulation. Jour. Geoph. Res., 100, C7, 13, 515-13, 538.

7 Figure captions

Figure 1: Scatter plot of DIN annual means obtained with run b9 vs b14, b11, and b10 at 100m (plot a,b and c) and at 300m (plot d,e, and f) depth respectively.The Levantine and the Ionian values are marked with light and dark gray, the Western Mediterrean values are plotted in black.

Figure 2: a) Annual means of the total transport streamfunction (Sv); b) DIN concentration at 140m ($mmolNm^{-3}$) superimposed with the streamlines of the velocity vertically integrated above this quota

Figure 3: Scatter plot of total transport streamfunction (Sv) in abscissa vs DIN concentration ($mmolNm^{-3}$) in ordinates respectively at 40m (a), 100m (b), 180m (c) and 300m (d) depth

Figure 4: DIN distribution in February(a), June(b), September(c) and December(d) at 60m depth ($mmolNm^{-3}$)

Figure 5: DIN distribution in February(a), June(b), September(c) and December(d) at 180m depth ($mmolNm^{-3}$)

Figure 6: Annual mean of the difference of the DIN concentration at 180m depth between b10.567 (high detritus flux) and b9.567 (low detritus flux) expressed in $mmolNm^{-3}$

Figure 7: First, second and third year Hovmoller Diagram (run 14) in a sample station in Ligurian Sea (44.25N 9E); DIN contoured-phytoplankton shaded above ($mmolNm^{-3}$); temperature contoured-salinity shaded beneath

Figure 8: First, second and third year Hovmoller Diagram (run 14) in a sample station in Balearic Sea (39N 6E); DIN contoured-phytoplankton shaded above ($mmolNm^{-3}$); temperature contoured-salinity shaded beneath

Figure 9: First, second and third year Hovmoller Diagram (run 14) in a sample station in Ionian Sea (34N 19E); DIN contoured-phytoplankton shaded above ($mmolNm^{-3}$); temperature contoured-salinity shaded beneath

Figure 10: First, second and third year Hovmoller Diagram (run 14) in a sample station in Levantine Basin (34N 34E); DIN contoured-phytoplankton shaded above ($mmolNm^{-3}$); temperature contoured-salinity shaded beneath

Figure 11: Chlorophyll concentration in April and in October for the first 20m ($mgChlm^{-3}$)

Figure 12: Chlorophyll surface concentration in April and in October obtained from the CZCS data for the years 1978-1986 ($mgChlm^{-3}$)

Figure 13: Chlorophyll concentration in January and July for the first 20m ($mgChlm^{-3}$)

Figure 14: Chlorophyll surface concentration in January and in July obtained from the CZCS data for the years 1978-1986 ($mgChlm^{-3}$)

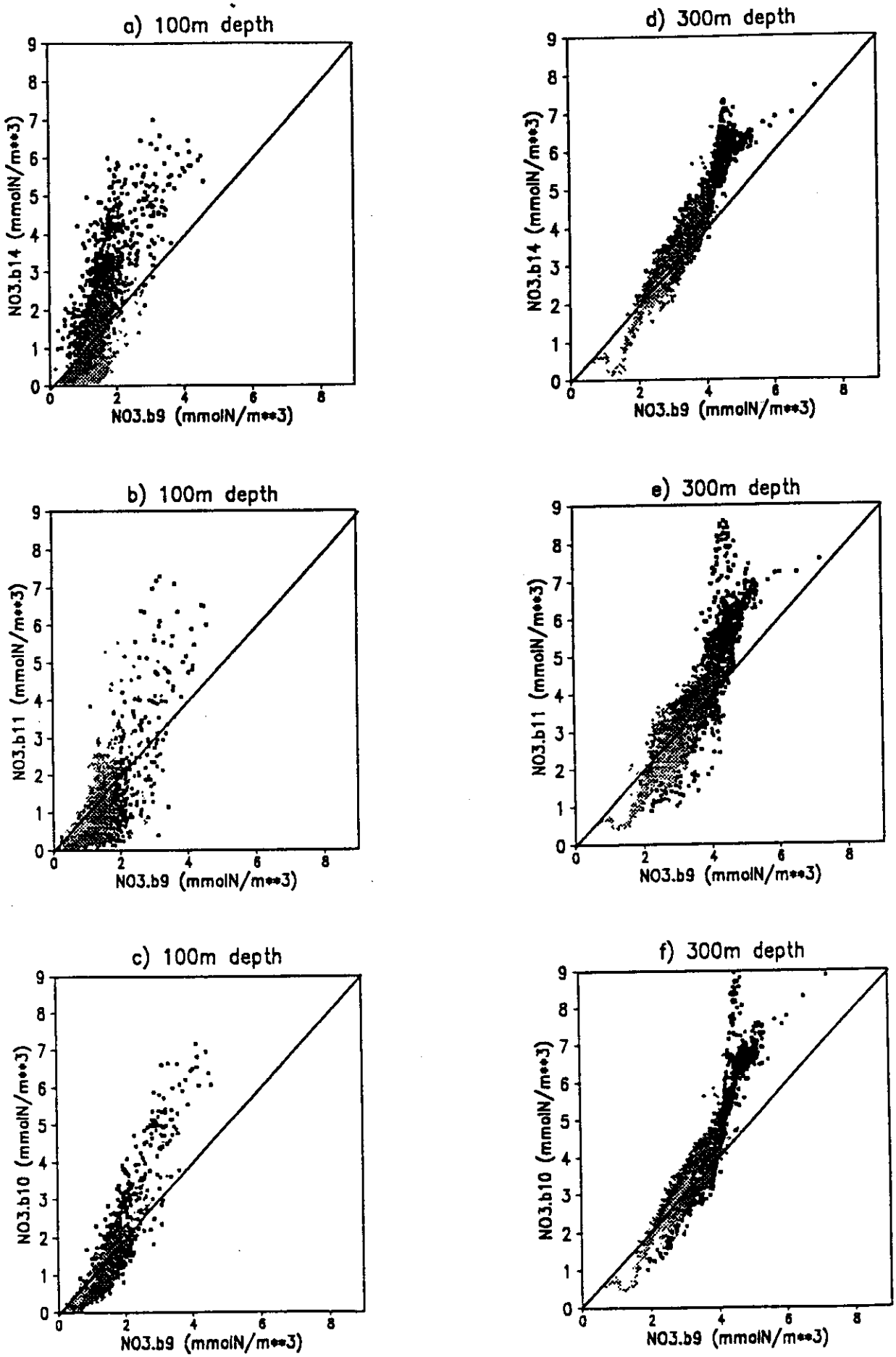
a) 100m depth
NO3.b14 (mmolN/m**3)
NO3.b9 (mmolN/m**3)
d) 300m depth
NO3.b14 (mmolN/m**3)
NO3.b9 (mmolN/m**3)
b) 100m depth
NO3.b11 (mmolN/m**3)
NO3.b9 (mmolN/m**3)
e) 300m depth
NO3.b11 (mmolN/m**3)
NO3.b9 (mmolN/m**3)
c) 100m depth
NO3.b10 (mmolN/m**3)
NO3.b9 (mmolN/m**3)
f) 300m depth
NO3.b10 (mmolN/m**3)
NO3.b9 (mmolN/m**3)

Fig. 1

Annual Mean Transport Streamfunction

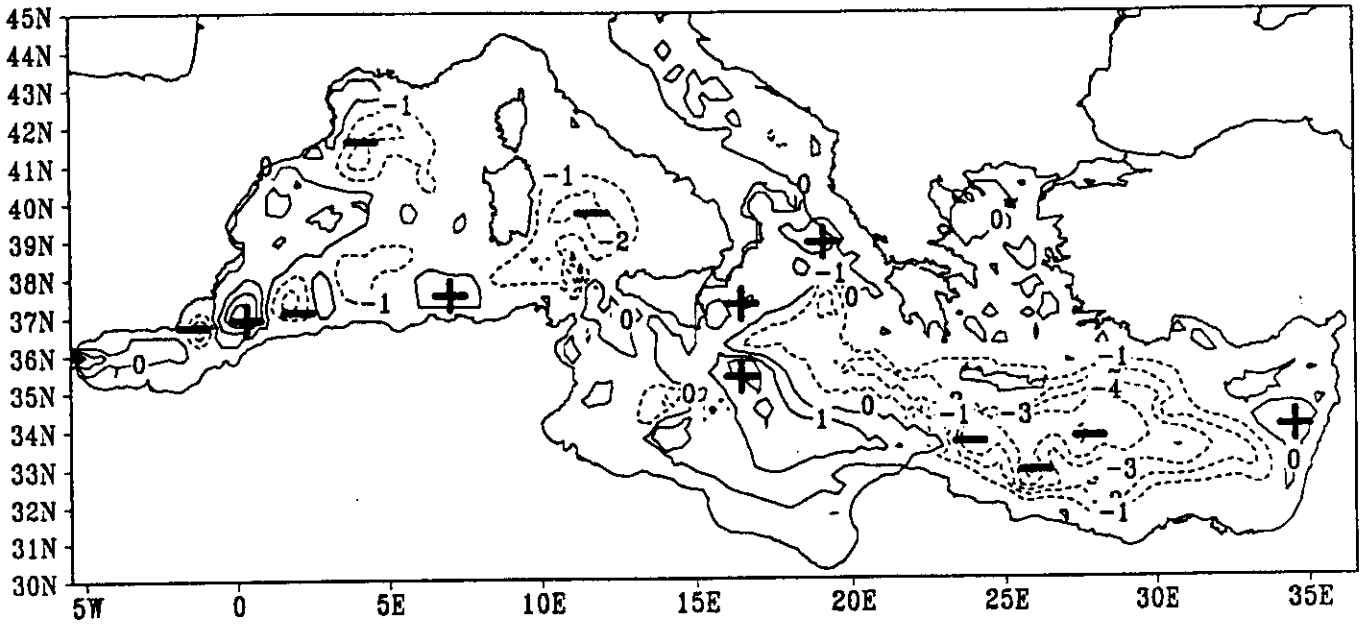

Annual Mean N03 Concentration at 140m

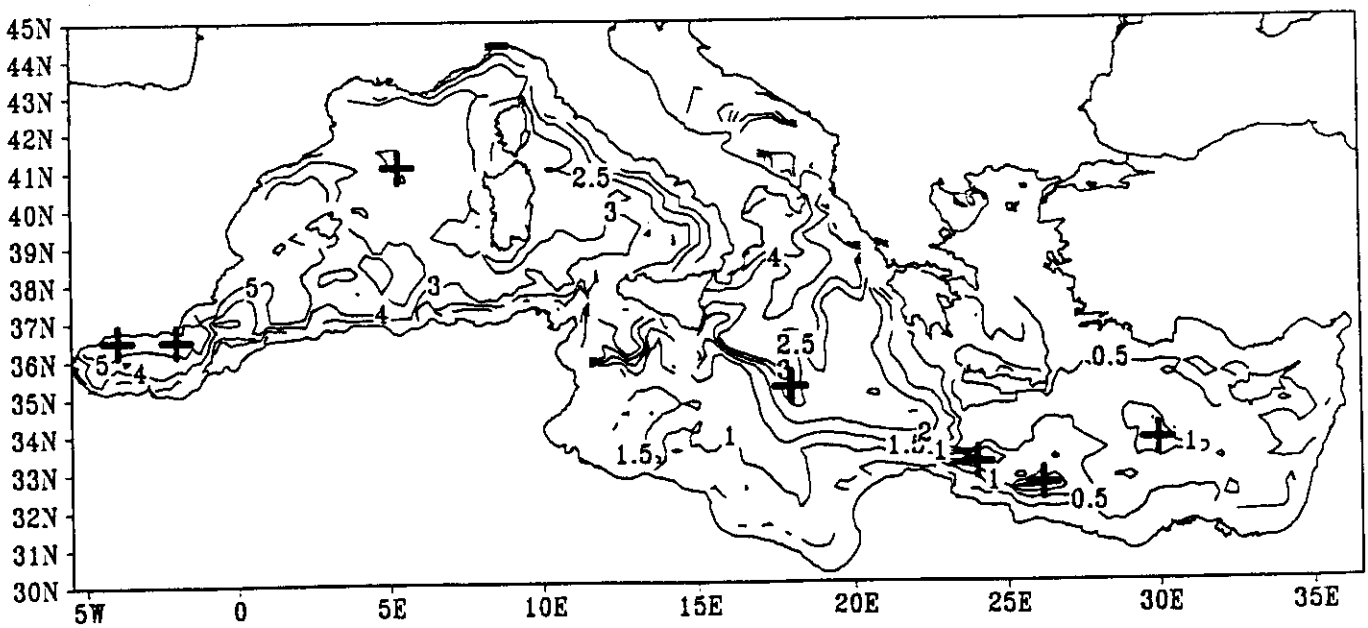

Fig. 2

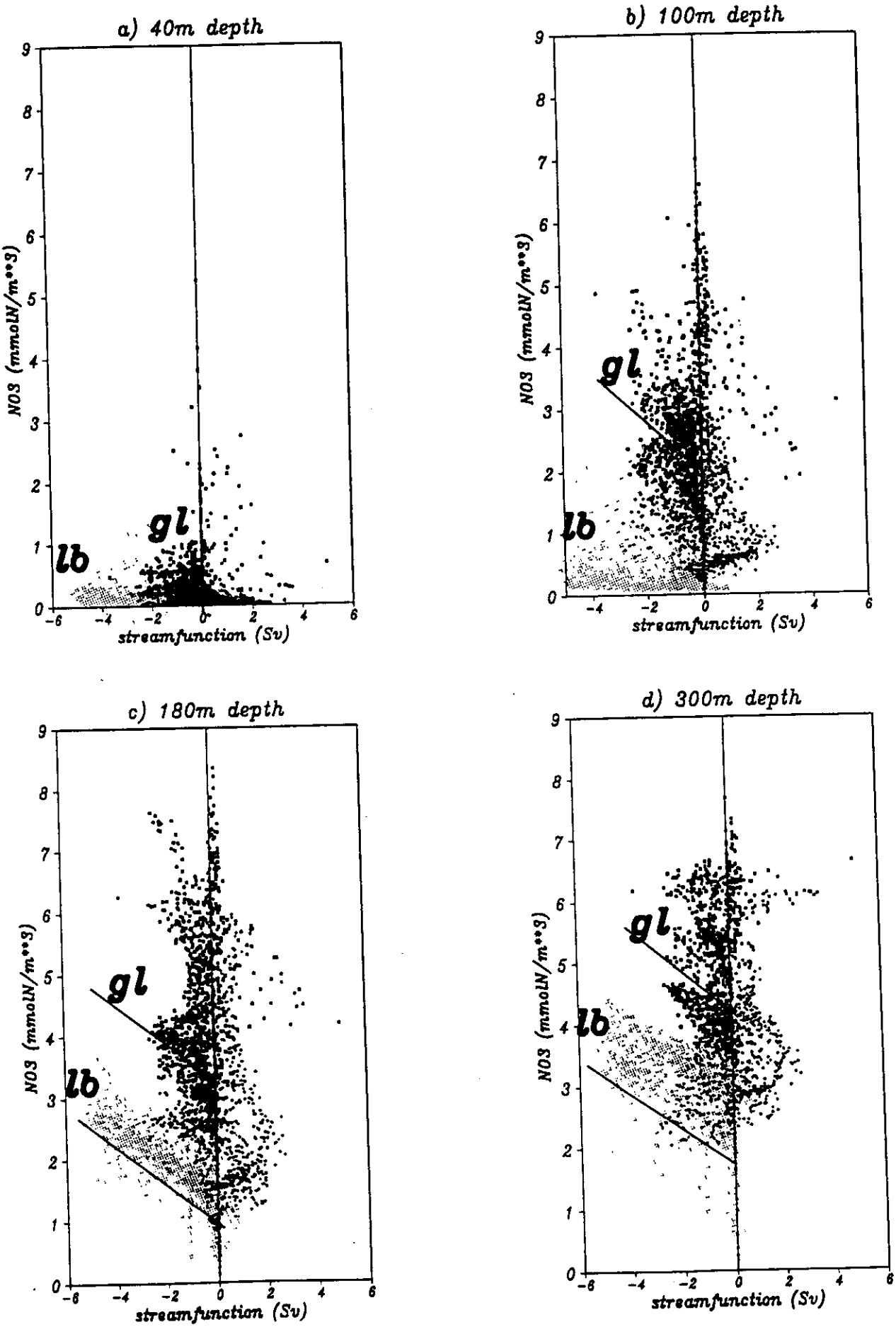
a) 40m depth
b) 100m depth
c) 180m depth
d) 300m depth
NO3 (mmolN/m**3)
streamfunction (Sv)
gl
lb

Fig. 3

NO3 concentration (mmolN/m**3) at 60m

a) February

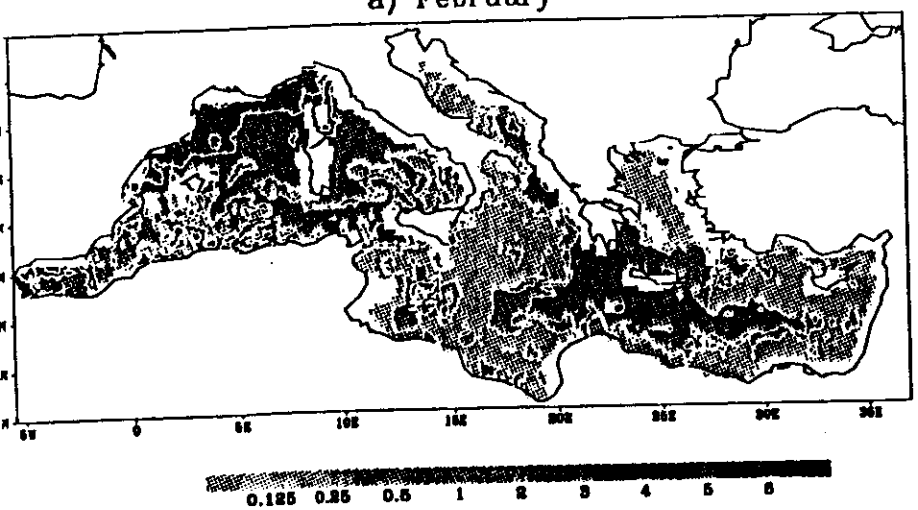

c) September

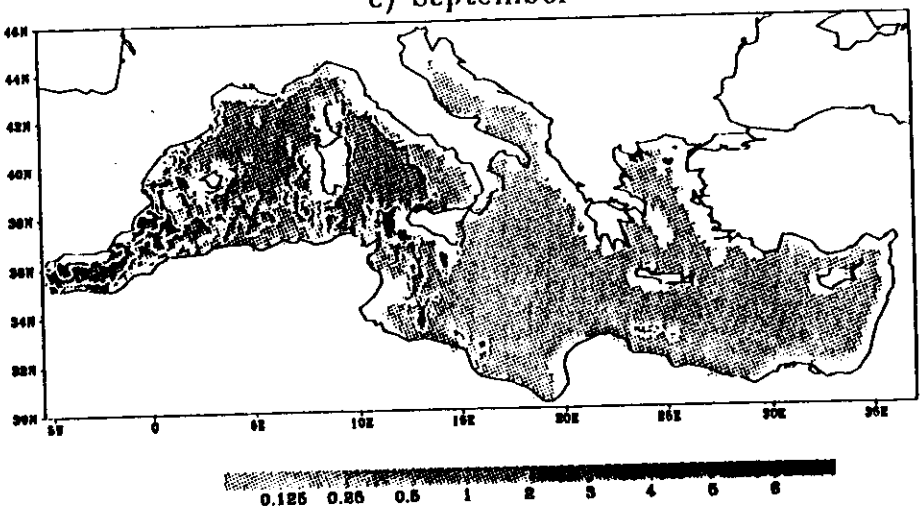

b) June

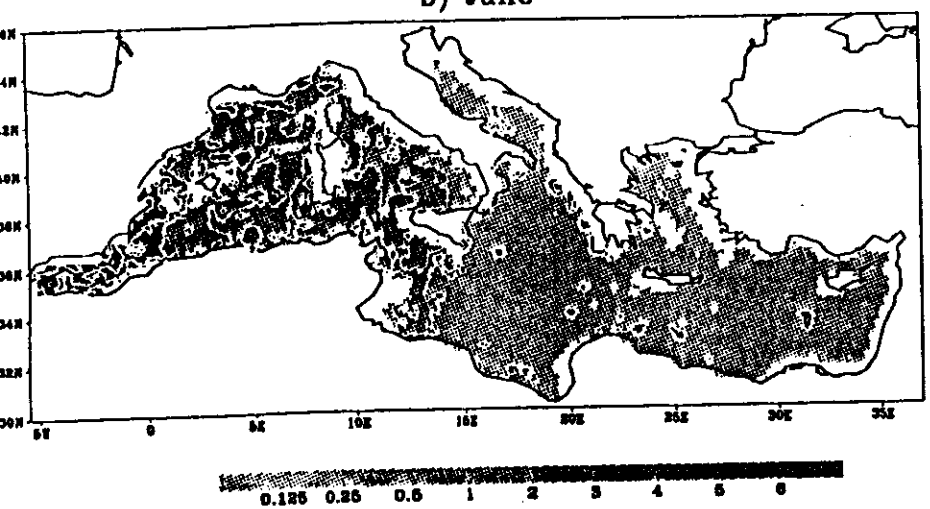

d) December

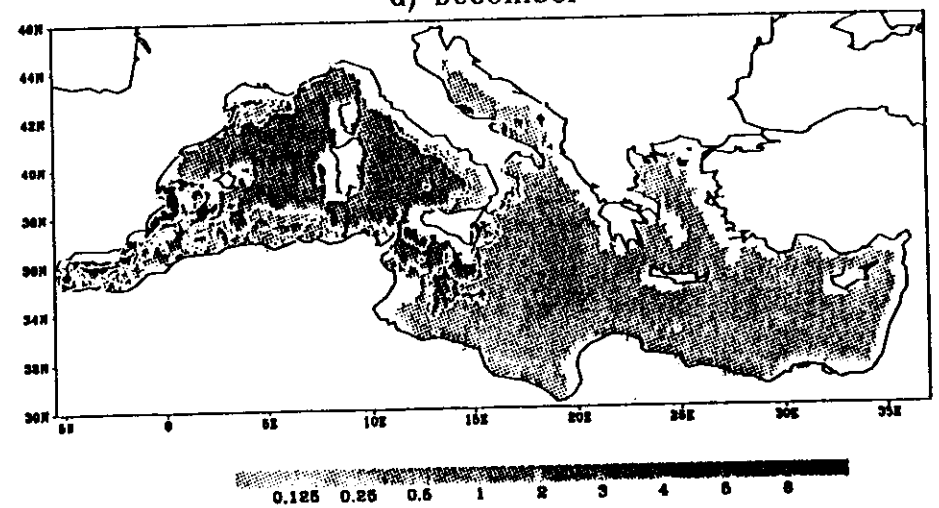

Fig. 5

Fig. 5b

NO3 concentration (mmolN/m**3) at 180m

a) February

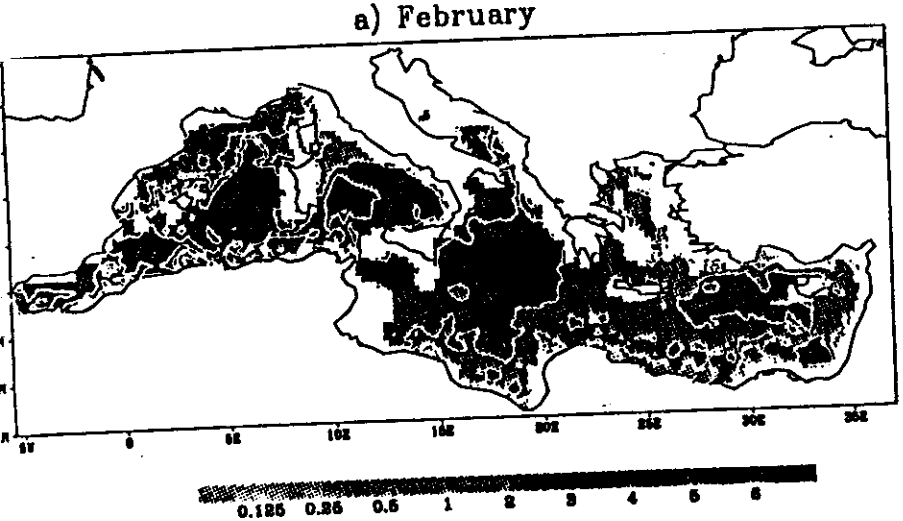

c) September

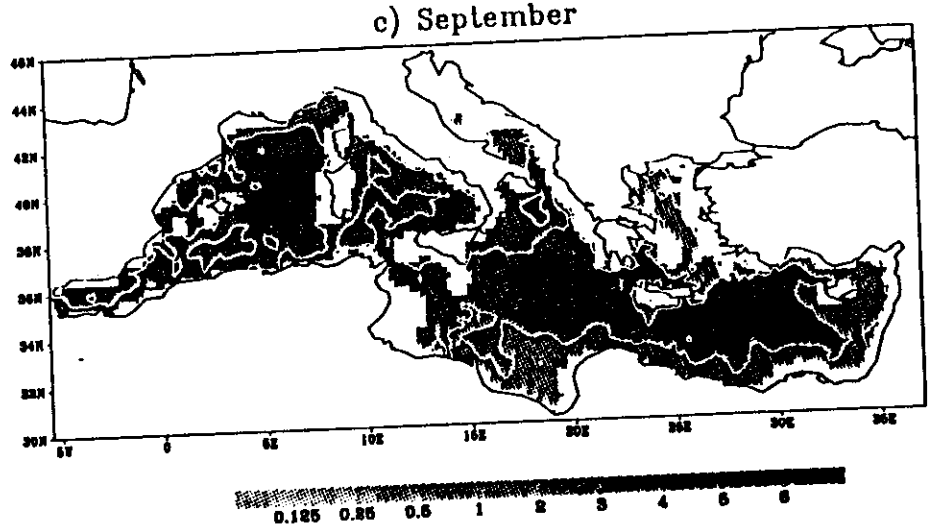

b) June

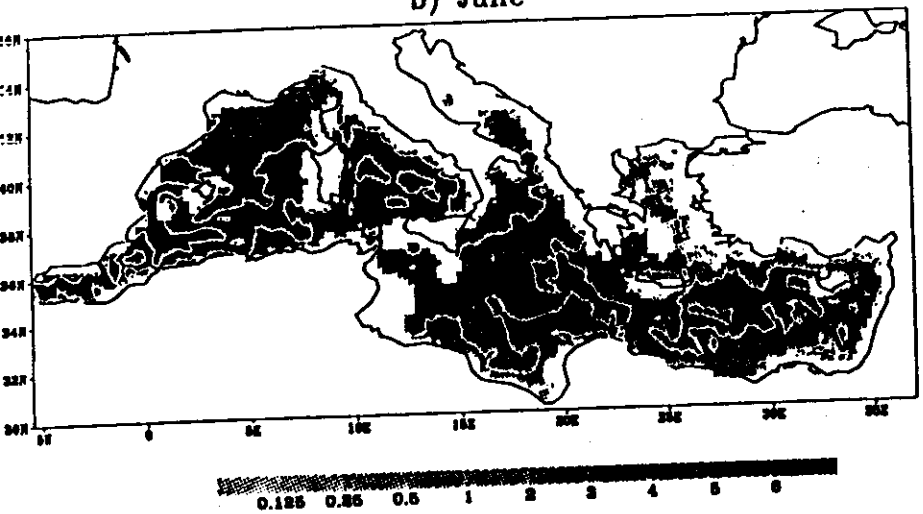

d) December

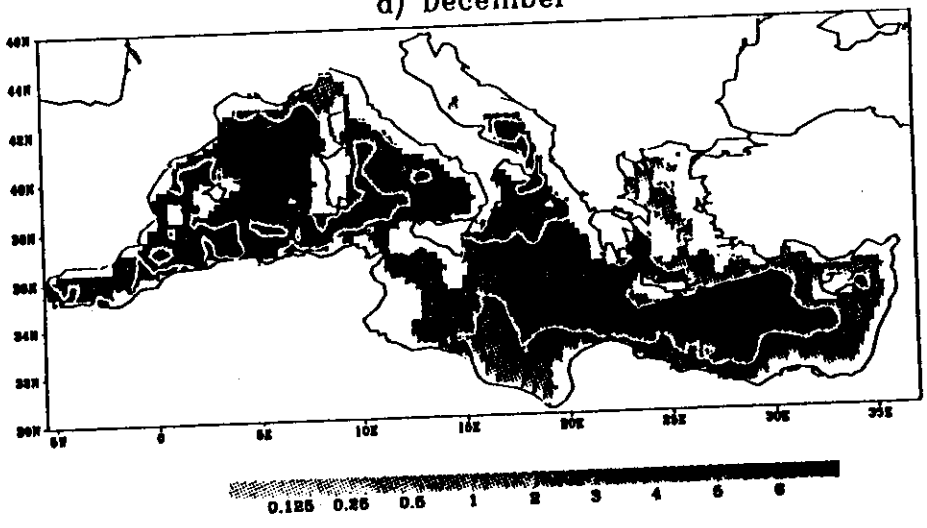

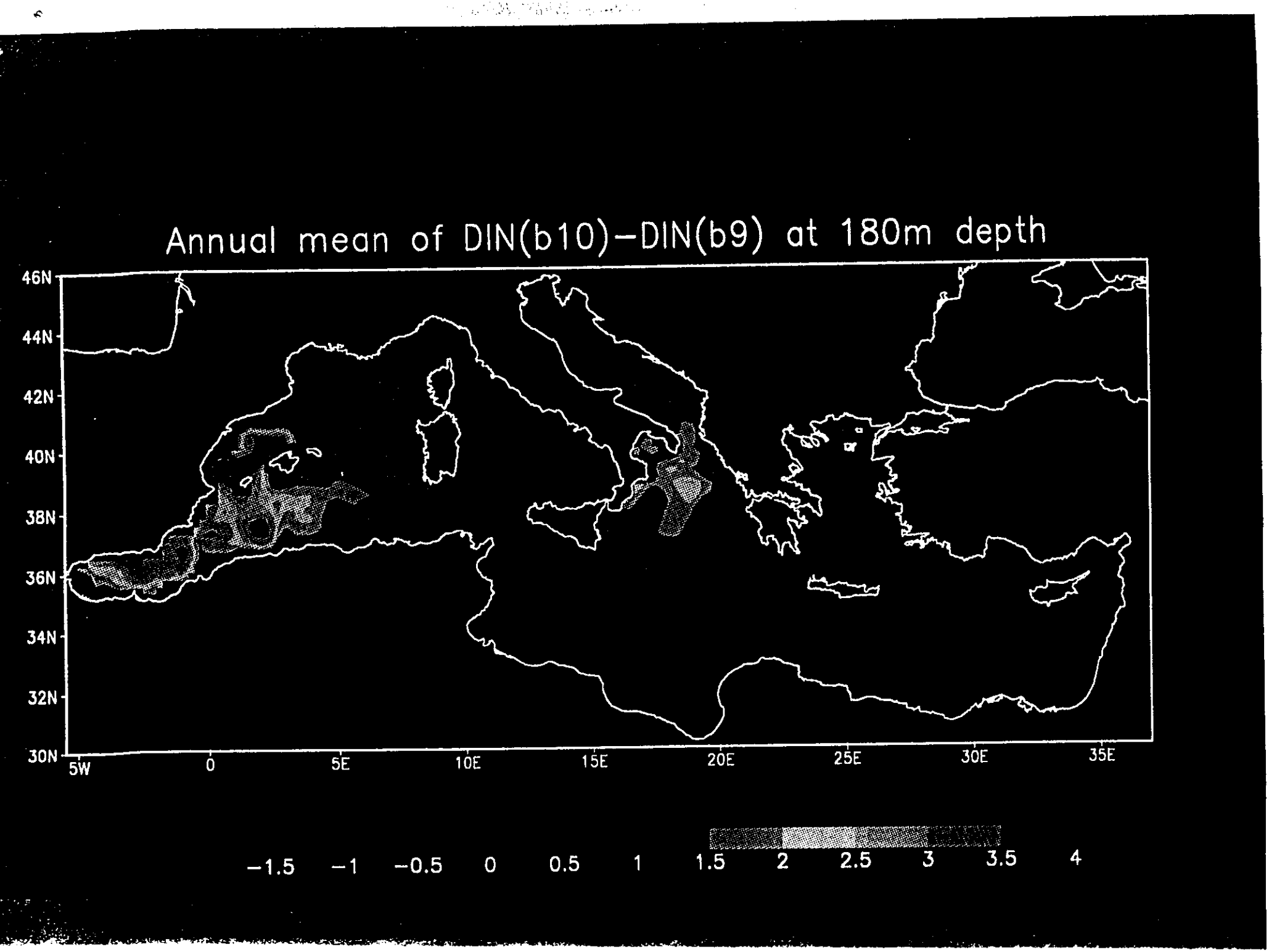
Annual mean of DIN(b10)−DIN(b9) at 180m depth
46N
44N
42N
40N
38N
36N
34N
32N
30N
5W
0
5E
10E
15E
20E
25E
30E
35E
−1.5
−1
−0.5
0
0.5
1
1.5
2
2.5
3
3.5
4

Fig. 6

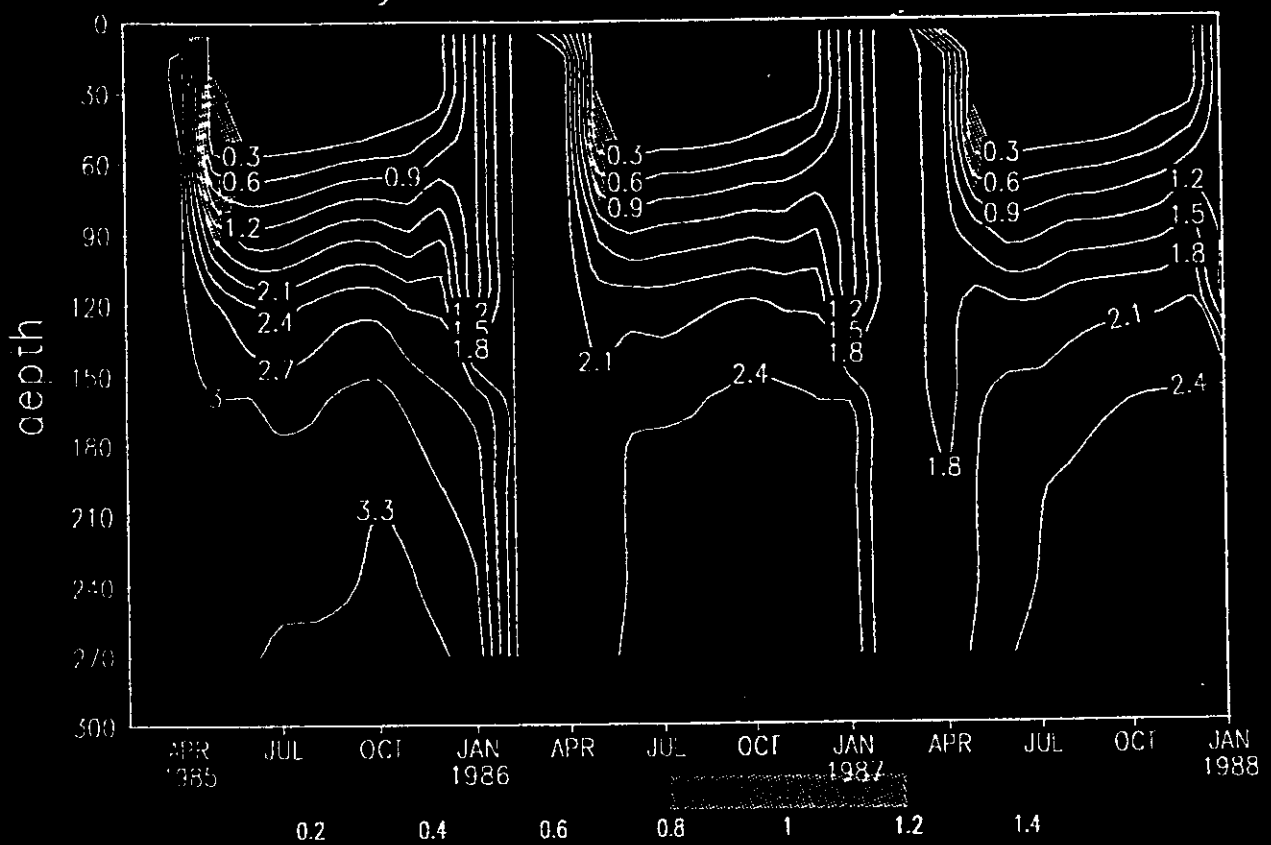
DIN–Phyto – St. 44.25N 9E run 14
depth
0
30
60
90
120
150
180
210
240
270
300
0.3
0.6
0.9
1.2
1.5
1.8
2.1
2.4
2.7
3.3
APR 1985
JUL
OCT
JAN 1986
APR
JUL
OCT
JAN 1987
APR
JUL
OCT
JAN 1988
0.2
0.4
0.6
0.8
1
1.2
1.4

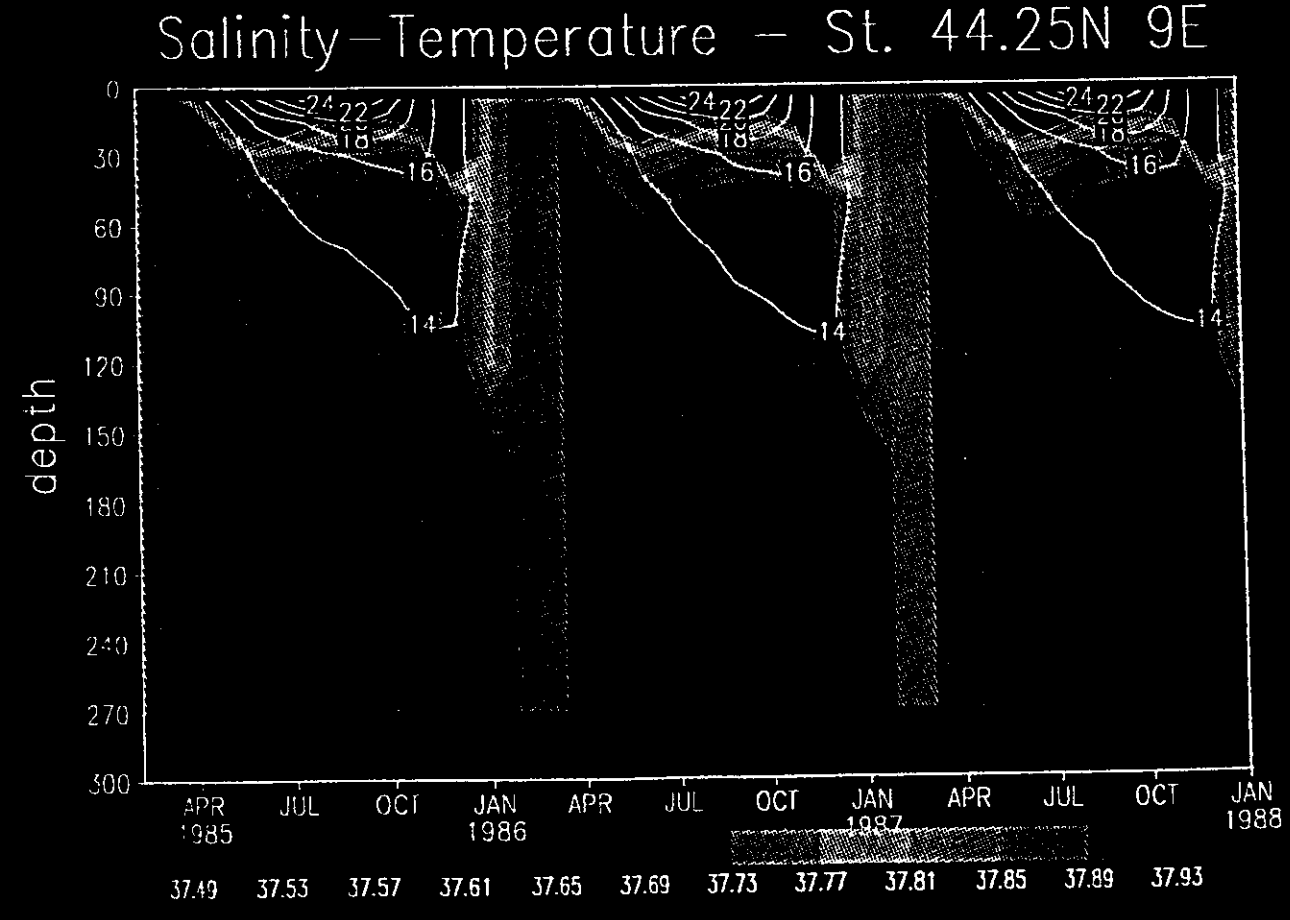
Salinity–Temperature – St. 44.25N 9E
depth
0
30
60
90
120
150
180
210
240
270
300
24
22
20
18
16
14
APR 1985
JUL
OCT
JAN 1986
APR
JUL
OCT
JAN 1987
APR
JUL
OCT
JAN 1988
37.49
37.53
37.57
37.61
37.65
37.69
37.73
37.77
37.81
37.85
37.89
37.93

Fig. 7

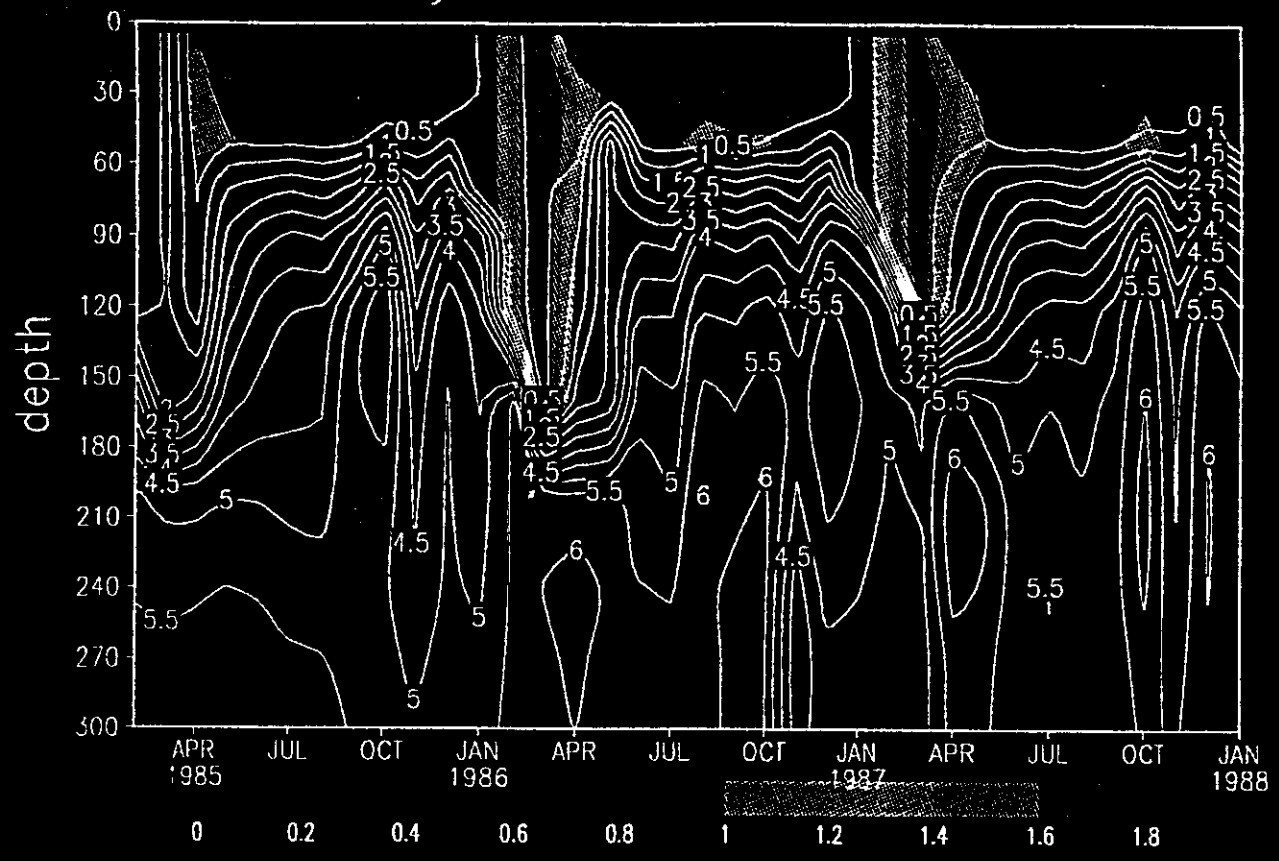
DIN–Phyto – St. 39N 6E run 14
depth
0
30
60
90
120
150
180
210
240
270
300
APR 1985
JUL
OCT
JAN 1986
APR
JUL
OCT
JAN 1987
APR
JUL
OCT
JAN 1988
0
0.2
0.4
0.6
0.8
1
1.2
1.4
1.6
1.8

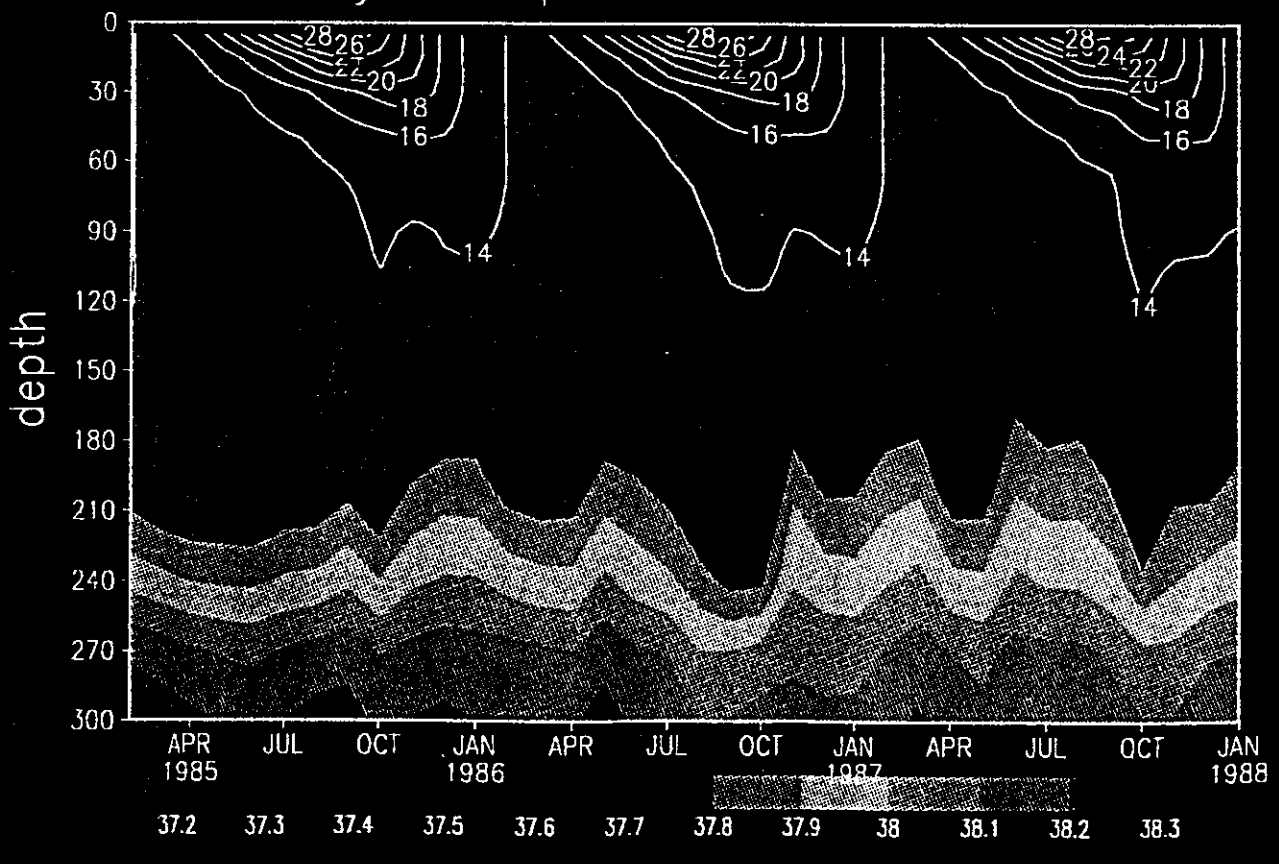
Salinity–Temperature – St. 39N 6E
depth
0
30
60
90
120
150
180
210
240
270
300
APR 1985
JUL
OCT
JAN 1986
APR
JUL
OCT
JAN 1987
APR
JUL
OCT
JAN 1988
37.2
37.3
37.4
37.5
37.6
37.7
37.8
37.9
38
38.1
38.2
38.3

Fig 8

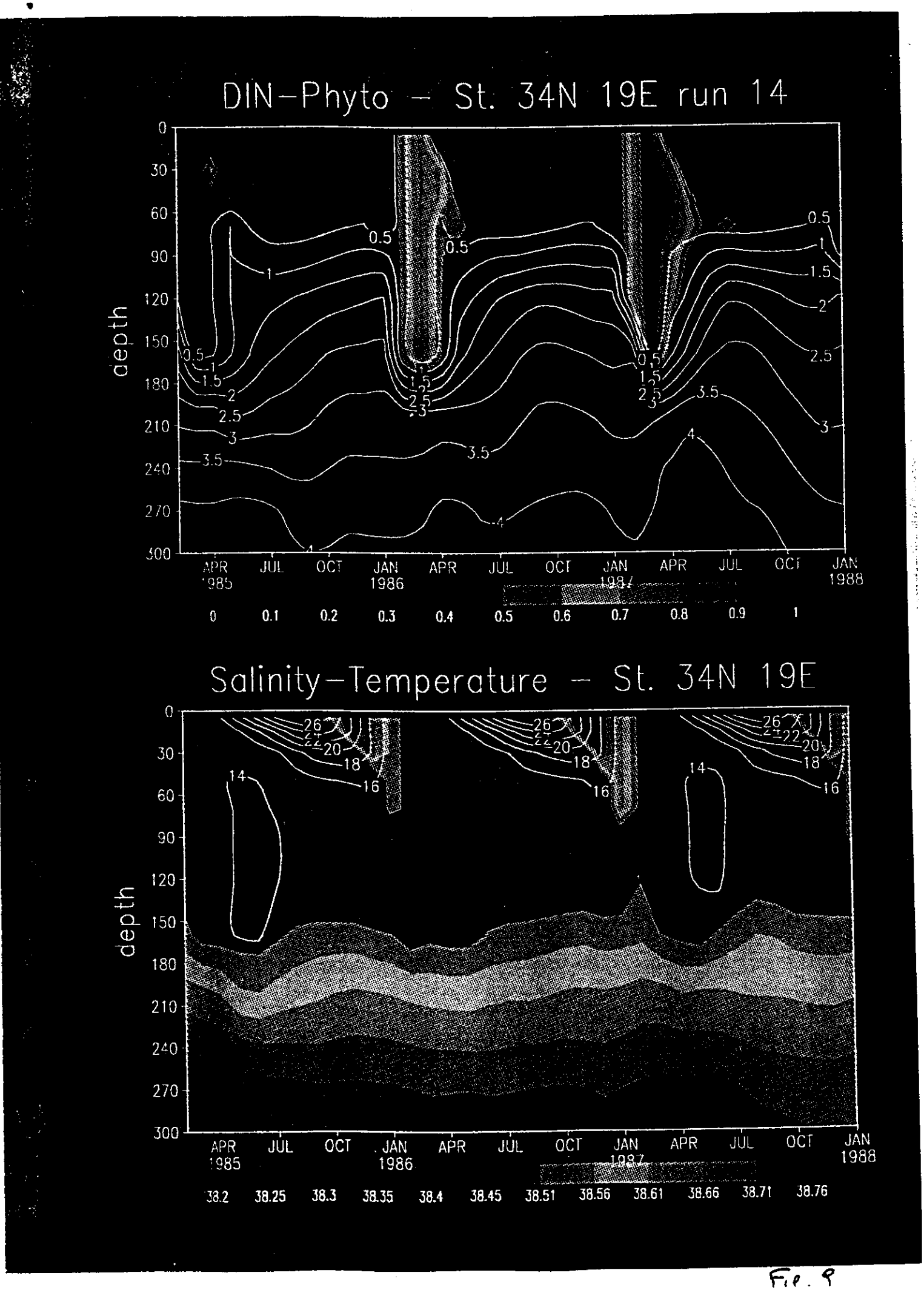
DIN–Phyto – St. 34N 19E run 14
depth
0
30
60
90
120
150
180
210
240
270
300
APR 1985
JUL
OCT
JAN 1986
APR
JUL
OCT
JAN 1987
APR
JUL
OCT
JAN 1988
0 0.1 0.2 0.3 0.4 0.5 0.6 0.7 0.8 0.9 1
Salinity–Temperature – St. 34N 19E
depth
APR 1985
JUL
OCT
JAN 1986
APR
JUL
OCT
JAN 1987
APR
JUL
OCT
JAN 1988
38.2 38.25 38.3 38.35 38.4 38.45 38.51 38.56 38.61 38.66 38.71 38.76

Fig. 9

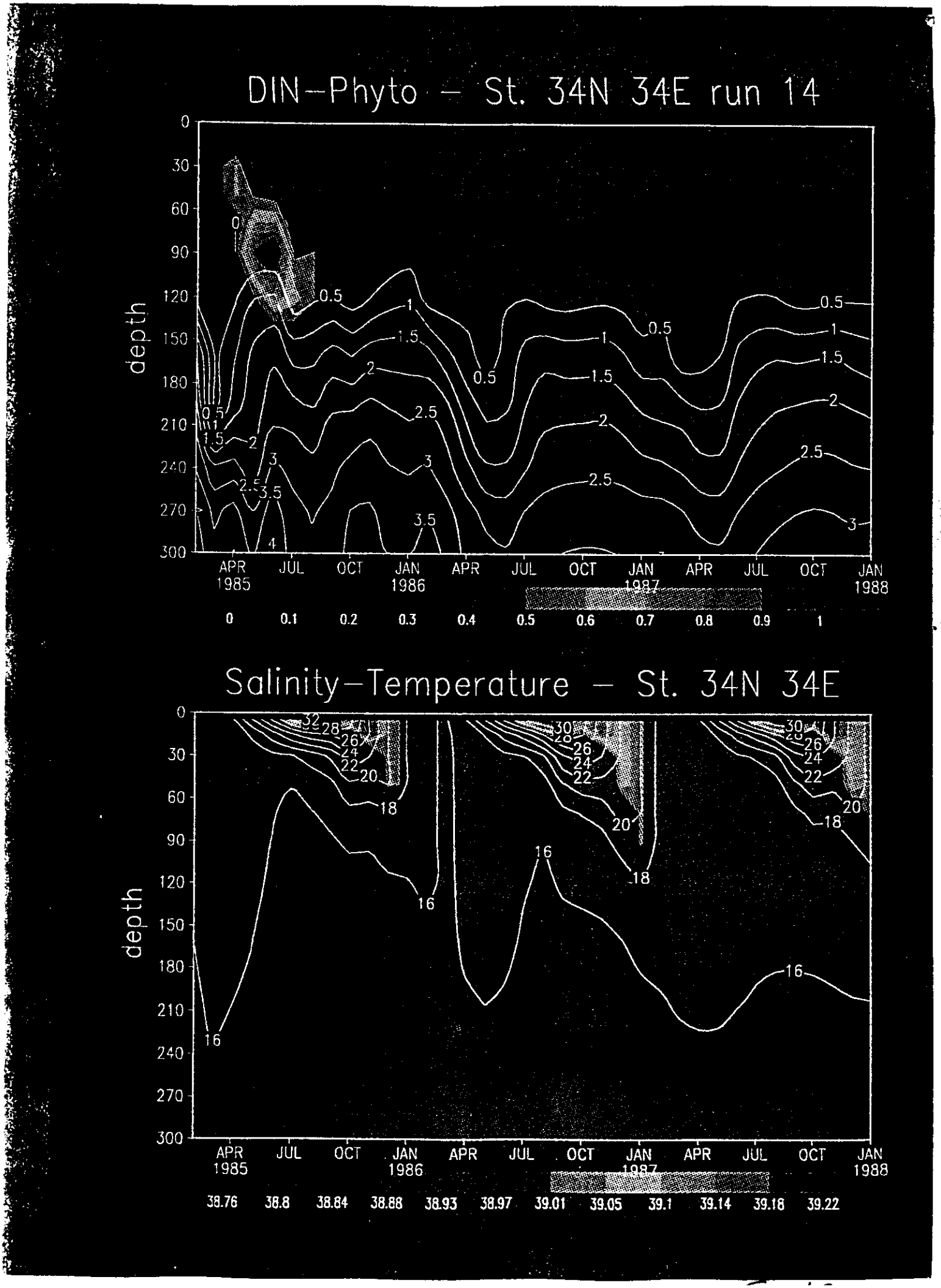
DIN–Phyto – St. 34N 34E run 14
depth
0
30
60
90
120
150
180
210
240
270
300
APR 1985
JUL
OCT
JAN 1986
APR
JUL
OCT
JAN 1987
APR
JUL
OCT
JAN 1988
0 0.1 0.2 0.3 0.4 0.5 0.6 0.7 0.8 0.9 1
Salinity–Temperature – St. 34N 34E
depth
APR 1985
JUL
OCT
JAN 1986
APR
JUL
OCT
JAN 1987
APR
JUL
OCT
JAN 1988
38.76 38.8 38.84 38.88 38.93 38.97 39.01 39.05 39.1 39.14 39.18 39.22

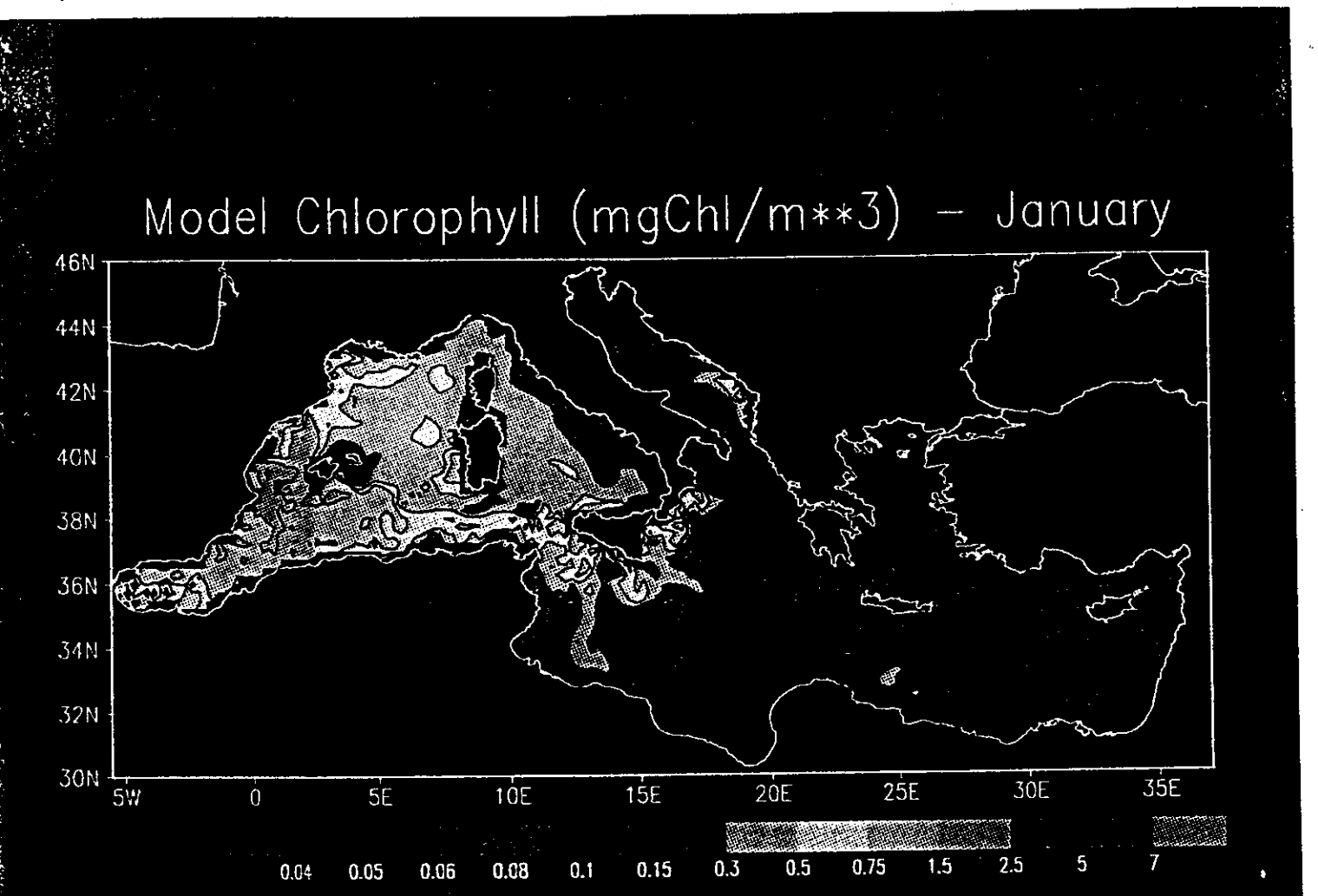
Model Chlorophyll (mgChl/m**3) - January
46N
44N
42N
40N
38N
36N
34N
32N
30N
5W
0
5E
10E
15E
20E
25E
30E
35E
0.04
0.05
0.06
0.08
0.1
0.15
0.3
0.5
0.75
1.5
2.5
5
7

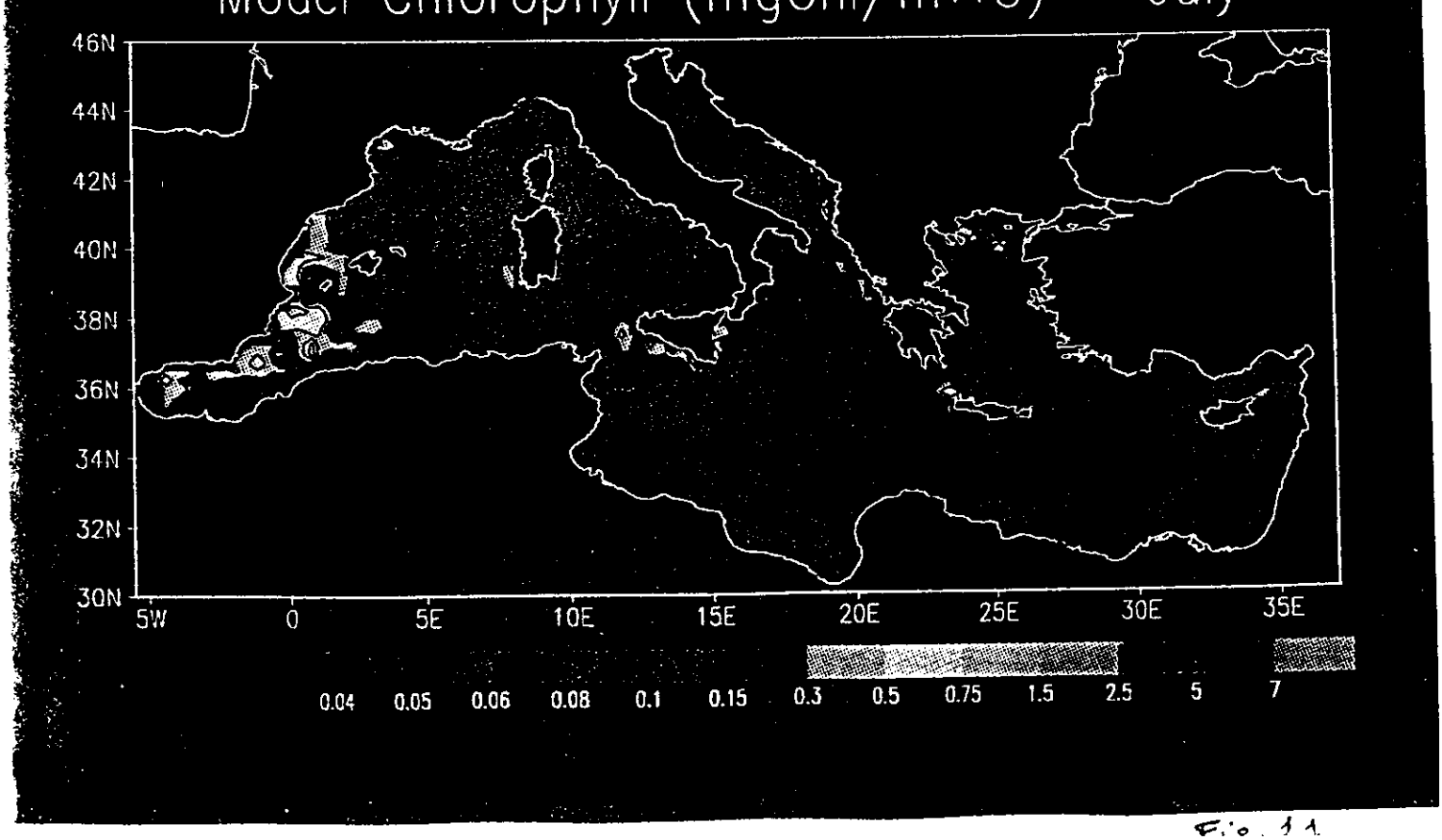
Model Chlorophyll (mgChl/m**3) - July
46N
44N
42N
40N
38N
36N
34N
32N
30N
5W
0
5E
10E
15E
20E
25E
30E
35E
0.04
0.05
0.06
0.08
0.1
0.15
0.3
0.5
0.75
1.5
2.5
5
7

Fig. 11

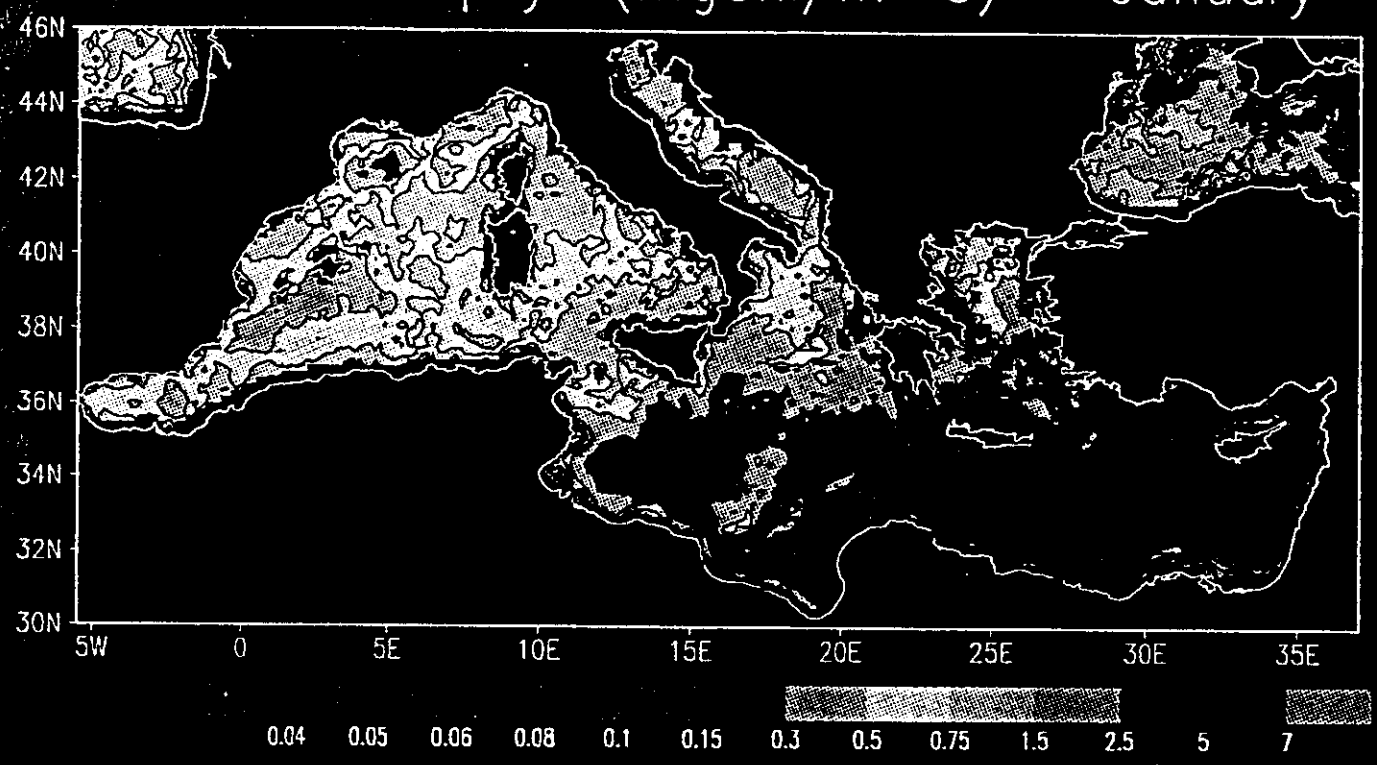
CZCS Chlorophyll (mgChl/m**3) – January
46N
44N
42N
40N
38N
36N
34N
32N
30N
5W
0
5E
10E
15E
20E
25E
30E
35E
0.04
0.05
0.06
0.08
0.1
0.15
0.3
0.5
0.75
1.5
2.5
5
7

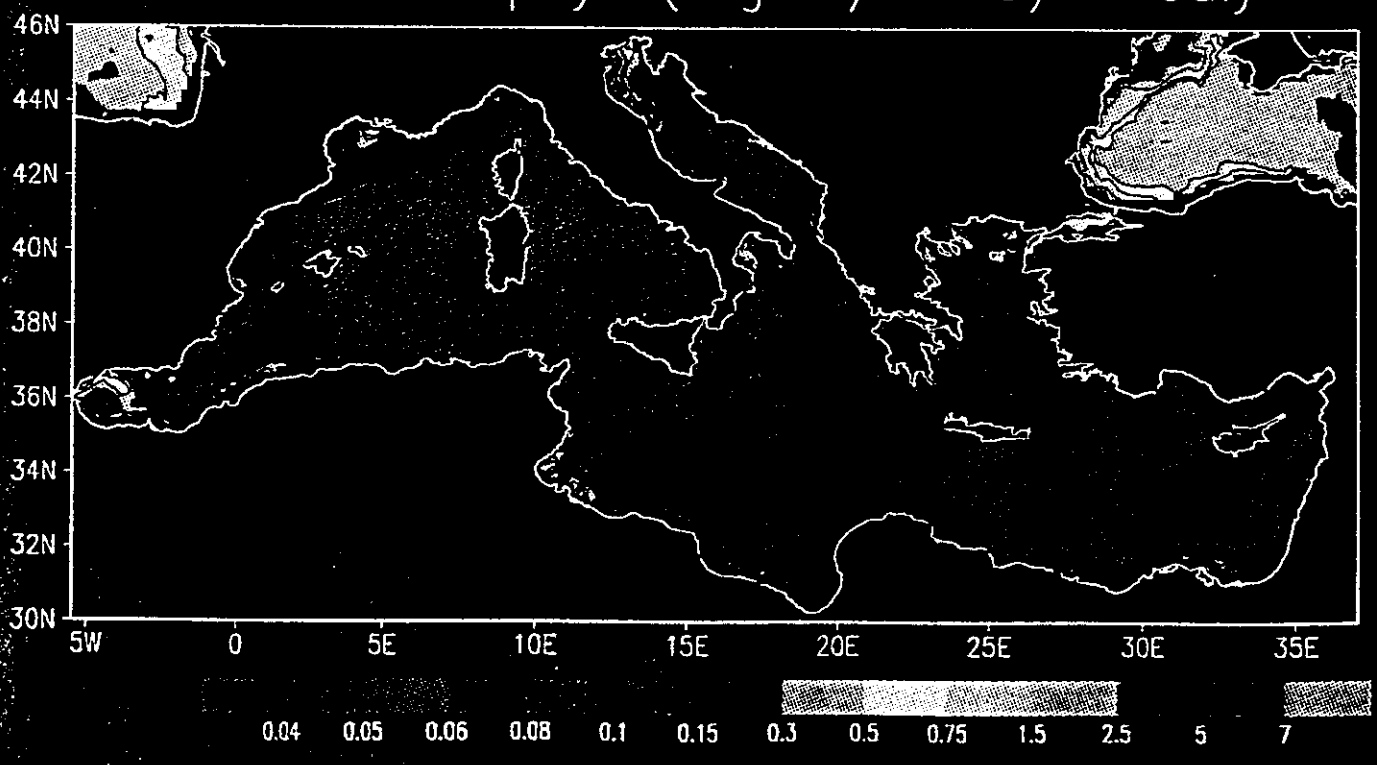
CZCS Chlorophyll (mgChl/m**3) – July
46N
44N
42N
40N
38N
36N
34N
32N
30N
5W
0
5E
10E
15E
20E
25E
30E
35E
0.04
0.05
0.06
0.08
0.1
0.15
0.3
0.5
0.75
1.5
2.5
5
7

Fig. 12

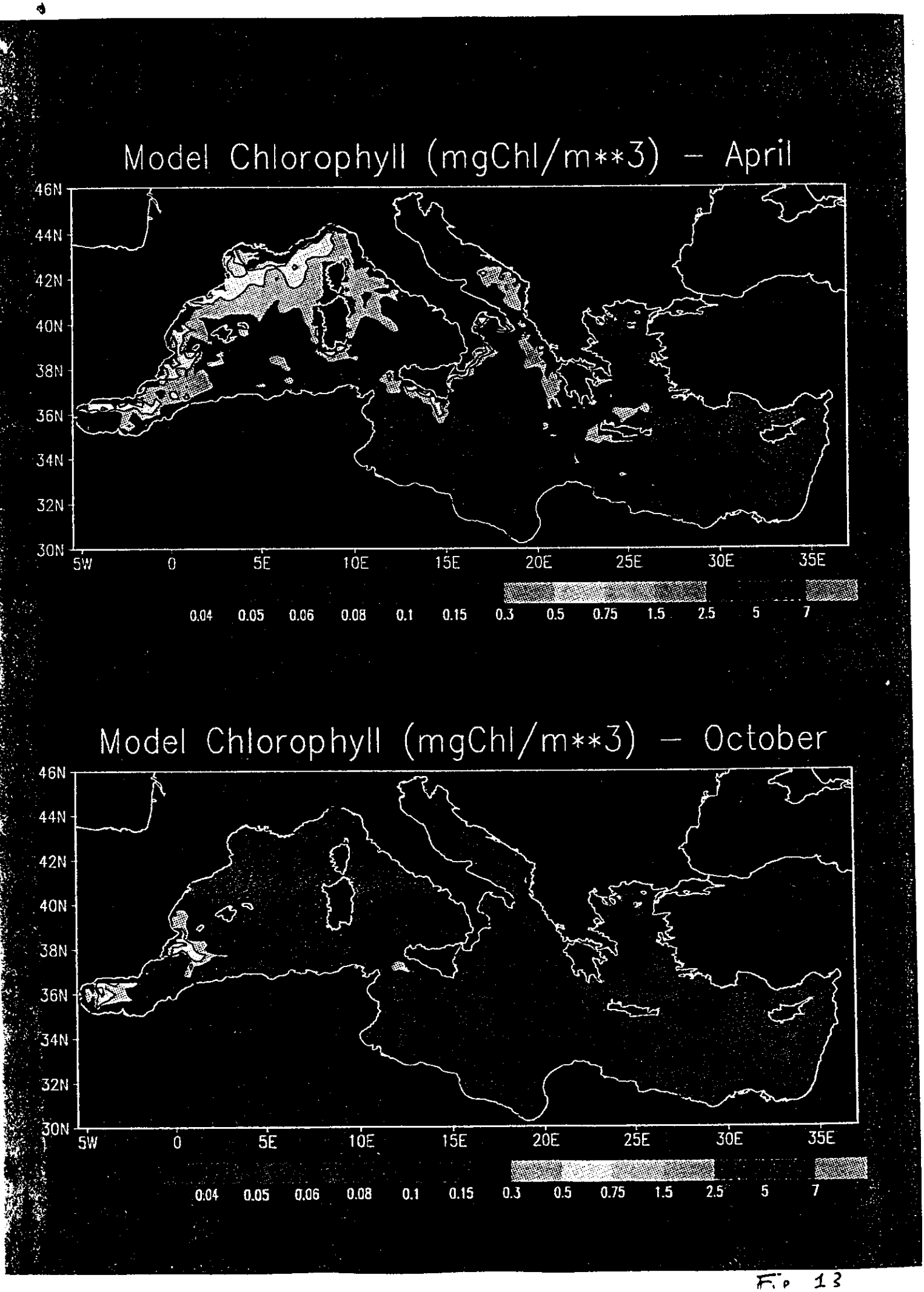
Model Chlorophyll (mgChl/m**3) – April
46N
44N
42N
40N
38N
36N
34N
32N
30N
5W
0
5E
10E
15E
20E
25E
30E
35E
0.04
0.05
0.06
0.08
0.1
0.15
0.3
0.5
0.75
1.5
2.5
5
7
Model Chlorophyll (mgChl/m**3) – October
46N
44N
42N
40N
38N
36N
34N
32N
30N
5W
0
5E
10E
15E
20E
25E
30E
35E
0.04
0.05
0.06
0.08
0.1
0.15
0.3
0.5
0.75
1.5
2.5
5
7

Fig 13

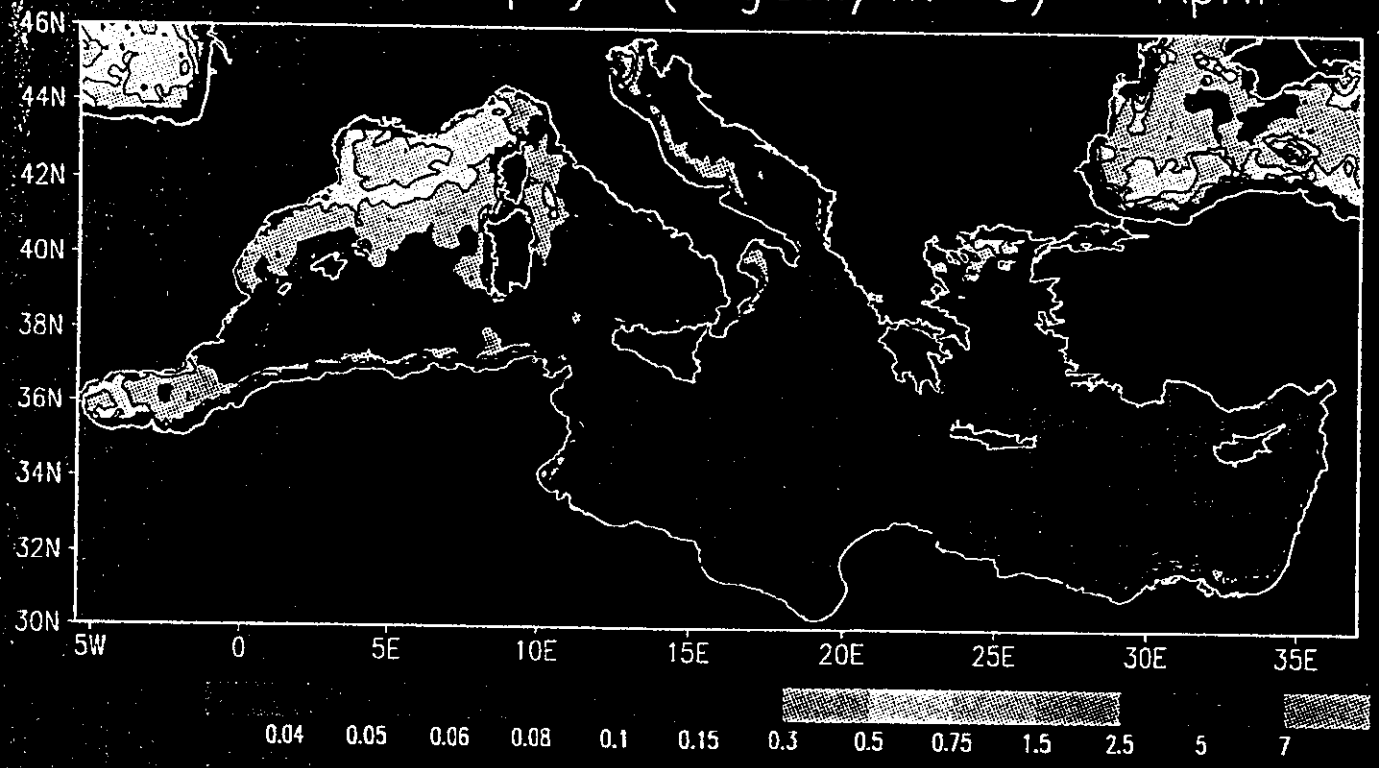
CZCS Chlorophyll (mgChl/m**3) - April
46N
44N
42N
40N
38N
36N
34N
32N
30N
5W
0
5E
10E
15E
20E
25E
30E
35E
0.04
0.05
0.06
0.08
0.1
0.15
0.3
0.5
0.75
1.5
2.5
5
7

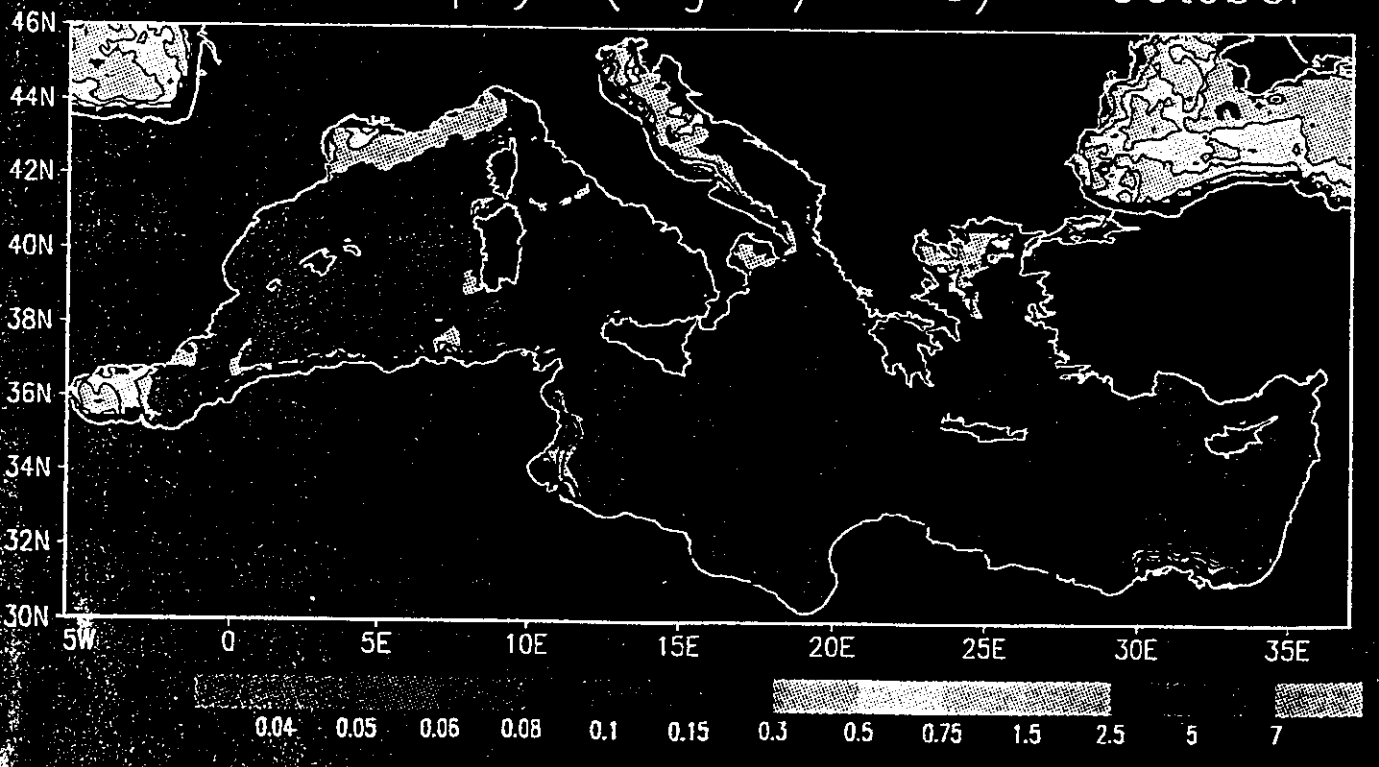
CZCS Chlorophyll (mgChl/m**3) - October
46N
44N
42N
40N
38N
36N
34N
32N
30N
5W
0
5E
10E
15E
20E
25E
30E
35E
0.04
0.05
0.06
0.08
0.1
0.15
0.3
0.5
0.75
1.5
2.5
5
7

Fig. 14